



Interpretation of interseismic deformations and the seismic cycle associated with large subduction earthquakes

Olga Trubienko^a, Luce Fleitout^{a,*}, Jean-Didier Garaud^b, Christophe Vigny^a

^a Laboratoire de Géologie, ENS, 24 rue Lhomond, 75231 Paris Cedex 05, France

^b Onera – The French Aerospace Lab, F-92322 Châtillon, France

ARTICLE INFO

Article history:

Received 12 December 2011

Received in revised form 22 December 2012

Accepted 26 December 2012

Available online 11 January 2013

Keywords:

Seismic cycle

Finite element

Subduction

Earthquake

Viscoelastic asthenosphere

Low viscosity wedge

ABSTRACT

The deformations of the overriding and subducting plates during the seismic cycle associated with large subduction earthquakes are modelled using 2D and 3D finite element techniques. A particular emphasis is put on the interseismic velocities and on the impact of the rheology of the asthenosphere.

The distance over which the seismic cycle perturbs significantly the velocities depends upon the ratio of the viscosity in the asthenosphere to the period of the seismic cycle and can reach several thousand km for rheological parameters deduced from the first years of deformation after the Aceh earthquake. For a same early postseismic velocity, a Burger rheology of the asthenosphere implies a smaller duration of the postseismic phase and thus smaller interseismic velocities than a Maxwell rheology. A low viscosity wedge (LVW) modifies very significantly the predicted horizontal and vertical motions in the near and middle fields. In particular, with a LVW, the peak in vertical velocity at the end of the cycle is predicted to be no longer above the deep end of the locked section of the fault but further away, above the continentward limit of the LVW.

The lateral viscosity variations linked to the presence at depth of the subducting slab affect substantially the results.

The north–south interseismic compression predicted by this preliminary 2D model over more than 1500 km within the Sunda block is in good agreement with the pre-2004 velocities with respect to South-China inferred from GPS observations in Thailand, Malaysia and Indonesia. In Japan, before the Tohoku earthquake, the eastern part of northern Honshu was subsiding while the western part was uplifting. This transition from subsidence to uplift so far away from the trench is well fitted by the predictions from our models involving a LVW.

Most of the results obtained here in a 2D geometry are shown to provide a good estimate of the displacements for fault segments of finite lateral extent, with a 3D spherical geometry, as long as the displacements during the seismic cycle are normalised by the coseismic displacement.

© 2013 Elsevier B.V. All rights reserved.

1. Introduction

Understanding the deformations in the subducting and overriding plates in areas subject to large subduction earthquakes is important for several issues concerning either natural hazards or our analysis of intraplate deformations: modelling stress accumulation in subduction zones is an important step towards the evaluation of seismic hazard in areas prone to large earthquakes. Through the analysis of interseismic deformations, mechanical models propose to distinguish the strongly and the weakly coupled zones (Chlieh et al., 2008) and to estimate the depth range over which the relative plate motion is blocked. These quantities are strongly linked to the potential moment of the earthquakes on the studied subduction segment.

The overriding and subducting plates are deformed coseismically rather far away from the trench (Vigny et al., 2005), but how large

are the deformations during the rest of the seismic cycle? Should one consider the strain rates measured by GPS during the last decades at some 1000 km from the trench as long-term geological strain rates or rather as consequences of the seismic cycle?

These strains linked to the seismic cycle may have important implications in terms of natural hazard: how could they affect the intraplate stresses and the seismicity (Ali and Freed, 2010; Delescluse et al., 2012; Pollitz et al., 1998)? A strong subsidence is observed in Thailand and Malaysia after the Sumatra earthquake, bringing fears about future flooding in the low-lying grounds of these countries (Satirapod et al., 2012). For how long is this post-seismic subsidence expected to continue?

One of the major problems of most models of the seismic cycle is that they are based either on scant data concerning the large earthquakes which occurred in the sixties or on the better measured signal linked to recent but smaller earthquakes. However, small earthquakes hardly affect the asthenosphere and it is very difficult to separate in the postseismic signal what is due to viscous relaxation

* Corresponding author. Tel.: +33 144322207.
E-mail address: fleitout@geologie.ens.fr (L. Fleitout).

from what comes from post-earthquake slip on the fault-plane. As a consequence, no consensus has been reached on these issues: the values of the viscosities proposed by models involving viscous relaxation in the asthenosphere are very dispersed: from 10^{20} Pa·s (Hu et al., 2004; Thatcher and Rundle, 1979) to 5×10^{17} Pa·s (Pollitz et al., 2006). Most models then have simply ignored any viscous relaxation.

Far-field motions measured by GPS after the 2004 Aceh giant earthquake are characterised by a strong postseismic horizontal signal, larger than the coseismic displacement after only four years, and by a strong subsidence (Panet et al., 2000; Pollitz et al., 1998; Satirapod et al., 2012). This subsidence is characteristic of relaxation in the asthenosphere and cannot be generated by slip on the bottom part of the fault. Fleitout et al. (2011), Satirapod et al. (2012) have been able to show that the rheology which is giving the best fit to the data is a Burger rheology with a transient viscosity close to 3×10^{18} Pa·s and a transient modulus about 3 times smaller than the seismic elastic coefficient. We found that power-law creep would not fit our data. In particular, the observed ratio of postseismic over coseismic deformations stays independent of the moment of the earthquake which induced them. The purpose of the present paper is to provide a view of the seismic cycle in the case of a viscoelastic asthenosphere with rheological properties corresponding to our inferences from the postseismic velocities after the Sumatra earthquake, trying to understand how the various details of the asthenospheric rheology and of the geometry in the subduction area affect the pattern of interseismic deformation and also how the displacements and associated quantities (stress) vary as function of time. We have restrained ourselves to a 2D Cartesian geometry in the first part of this study, to properly understand the principles and parameters influencing the deformations through the seismic cycle. Since lateral variations of viscosity linked to the slab or to the presence of a low viscosity wedge are considered, a finite element discretization method has been chosen.

In Section 2, the keypoints of various existing models for the seismic cycle are presented. Section 3 describes the finite-element 'realistic' model used in this study with an asthenosphere, plate velocities imposed in the far-field and periodic earthquakes; equivalent models which speed up the computations will be discussed in Appendix A. Section 4 discusses the impact on the seismic cycle of Burger versus Maxwell rheologies, of the locking depth on the interface, of the presence of a low viscosity wedge. In Section 5, the predictions from the above models are compared with those from the more commonly used elastic backslip models. We also discuss how neglecting the lateral viscosity variations linked to the slab at depth affect the results. In Section 6, we present a comparison of the predictions from our models with interseismic GPS data from Sumatra and adjacent areas and with vertical velocities in northern Honshu, Japan, before the Tohoku earthquake. Finally in Section 7 we use a 3D finite element model and discuss how the main results obtained from 2D models can be used in a 3D geometry.

2. Various models for the seismic cycle

Elastic or viscoelastic models of the seismic cycle have been put forward more than 30 years ago. Backslip is one of the most often used model for describing interseismic deformations (Savage and Prescott, 1978; Savage, 1983; Okada, 1985). The backslip method simply subtracts from the total motion the convergence motions, uniform in time and space for each plate, in order to keep only the variations linked to the seismic cycle. The seismic cycle is then described by two equal and opposite slidings on the seismogenic part of the subduction interface: abrupt coseismic slip during the earthquake and cumulative interseismic normal slip in the opposite direction, so-called "backslip". Although the first models (Savage, 1983; Thatcher and Rundle, 1979, 1984) considered the viscoelasticity of the mantle, the elastic backslip model has recently been the most often invoked (Dragert et al., 1994; Flück et al., 1997; Le Pichon et al., 1998; Okada, 1985; Savage et al.,

2000). The mantle is of course not elastic over long time-scales. The elastic backslip model is relevant only if the viscosity in the subduction region is everywhere sufficiently large so that the deformations can be considered as elastic at the time scale of the seismic cycle. Indeed, in this case, the 'plastic' deformation in the viscous parts of the system (asthenosphere, lower part of the subduction interface), which need to deform in order to accommodate the plate convergence, occurs at a constant rate and is not sensitive to the cyclic stress variations associated with the seismic cycle. Only the elastic deformations are then sensitive to the cyclic change of stress and can give rise to time-dependent strain rates.

Because of the limited distance range over which slip on a fault induces deformation in case of elastic rheology, most elastic backslip models only consider data at a rather small distance from the trench (<400 km) (for example, Simoes et al. (2004) and Chlieh et al. (2008)). As described in the early models (Savage, 1983; Thatcher and Rundle, 1979), if some part of the mantle has a sufficiently low viscosity (< 10^{20} Pa·s) so that it deforms significantly over the time-scale of the seismic cycle, the elastic model has no longer any reason to apply. After the earthquake, the viscous relaxation induces 'postseismic' motions in the same direction as the coseismic deformation. The interseismic phase which 'brings back to zero' during the seismic cycle the total displacements associated with co- and postseismic motions is then affected. The larger the postseismic phase, the stronger the difference between elastic and viscoelastic model predictions for the interseismic phase.

Note that the term 'interseismic' used here requires some definition: we will see that the post-seismic velocity induced by a single earthquake is expected to last for more than 100 years, decreasing asymptotically to zero over a very long period of time. As a consequence, the velocities keep on varying through the seismic cycle. The definition of 'interseismic' used here will simply refer to the velocities at the end of the cycle, just before the next earthquake.

Many models during the last 40 years proposed viscoelastic solutions based on the response to a dislocation in a layered or uniform viscoelastic medium, some considering only the postseismic response of a single earthquake, others considering the whole seismic cycle. There were first 2D Cartesian models with or without gravity (Savage, 1983; Thatcher and Rundle, 1979, 1984), bringing useful scaling laws and clarifying the role of various parameters such as 'locking depth over elastic thickness'. Many interesting analyses, in particular the non-dimensional parameters which govern the physics of postseismic deformations were presented in these early semi-analytical papers. Then 3D spherical viscoelastic models (compressible or incompressible) included all the physical effects important for low harmonics introduced in the normal-mode formulation (Nostro et al., 1999; Piersanti et al., 1995; Pollitz, 1997; Pollitz et al., 1998). Note that the lateral viscosity variations linked to the slab or to a low viscosity wedge are difficult to introduce in those models based on dislocation approaches. Attempts to introduce these lateral viscosity variations concluded that these were affecting very significantly the postseismic signal (Pollitz et al., 2008). It is why this problem has also been studied using finite element techniques, for example, in 2D by Melosh and Raefsky (1983) and in 3D by Freed et al. (2006), Wang et al. (2001) and Ali and Freed (2010). These last studies concentrated mainly on the deformation at a relatively short distance from the trench and thus did not address the same question as the present study. An interesting and didactic review concerning the seismic cycle has been published very recently (Wang et al., 2012). In particular, examples of displacement fields corresponding to various phases of the cycle are described in this paper.

3. Finite element model

To solve the problem of stress and strain distribution during the seismic cycle, we have used the finite element software Z-set/Zébulon (Z-set,

2011), employed here in its 2D version for most of the paper. The last section deals with a 3D geometry.

The geometrical model is schematically presented in Fig. 1. It is composed of the following main parts: an overriding plate and a subducting plate penetrating in the mantle down to 400 km depth, an asthenosphere between 80 and 200 km depth, a sub-asthenospheric mantle and, for some of the models, a low viscosity wedge. The modelled region is taken sufficiently large so that the seismic cycle does not induce any significant motion or deformation in the regions close to the mesh boundaries. Our solutions are then insensitive to the exact size of the modelled region (in practice, for most cases treated here, 4000 km on both sides of the trench is sufficient).

The domain is discretised by 6-nodes 2D triangular elements with plain strain formulation (Zienkiewicz and Taylor, 2000). As can be seen in Fig. 1, the mesh is refined near the fault to properly capture the strong variations of stress in this region; it is de-refined further away to keep an overall reasonable computational time.

The shear and bulk moduli increase with depth according to PREM in the whole model box. Both the overriding and subducting plates are modelled with a linear elastic behaviour. The asthenosphere has a viscoelastic behaviour, which is detailed in Appendix B. The mantle below the asthenosphere is represented by a Maxwell viscoelastic layer with viscosities increasing exponentially from 1.5×10^{19} Pa·s at 200 km depth to 3×10^{21} Pa·s at 670 km depth. It is maintained to 3×10^{21} Pa·s in the lower mantle (but the value of this viscosity has little influence on our results as long as it is sufficiently large). For the case with a 10^{20} Pa·s asthenosphere, the viscosity in the upper mantle below 200 km increases from 1.5×10^{20} Pa·s at 200 km depth to 3×10^{21} Pa·s at 670 km depth.

The nodes are duplicated along the subduction interface using the split node method (Melosh and Raefsky, 1981). To trigger a coseismic slip on the trench, the relative displacement of the coupled nodes are imposed tangentially on the interface.

Below this seismic zone, over the plate interface, the model includes a viscous channel to allow the plates to slide past each other. However, all the computations done here will correspond to the case where the viscosity in the channel is sufficiently high so that it behaves practically as an elastic material over the seismic cycle time-scale and this deep slip zone will play no role, except allowing finite relative plate velocities when we use the 'realistic' method (see Appendix A).

On the right and left boundaries, horizontal velocities are imposed or fixed to zero (see Appendix A). The bottom boundary condition corresponds to free slip and zero vertical velocity. No shear-stress is imposed on the top boundary; however, a vertical force equal to $-\rho \cdot g \cdot U_y^1$ is applied on this boundary in order to account (in a simplified way) for the gravitational forces due to vertical uplift or downlift.

In the following sections, results will be given in dimensional units and some of the rheological or geometrical parameters will be varied so that one understands their influence. However, through the non-dimensionalization of the mechanical equations, each of our numerical results can be used to understand the results for other sets of parameters (Thatcher and Rundle, 1984). For example, the results stay invariant if one multiplies by a same constant c the time (hence the period of the cycle) and the viscosity (the curves in displacement are the same but the velocities are divided by c if the coseismic displacement is fixed; the velocity curves are the same if the coseismic displacement is multiplied by c). All displacement or velocity values scale proportionally to the velocity between the two plates (here taken equal to 5.8 cm/yr) or more exactly to the proportion of this velocity accommodated by a succession of blocking periods followed by earthquakes. If there is partial coupling, then

the various quantities computed below should be multiplied by the coupling coefficient.

4. Response for various rheologies and geometries

To study the deformation and displacement field during the seismic cycle we use the viscoelastic finite element model described in Section 3. The most straightforward way to model the seismic cycle is to mimic what really occurs with plate convergence imposed in the far-field, earthquakes occurring periodically on the subduction interface and more or less high viscosities on the non-seismic part of the interface and in the asthenosphere to permit the long-term convergence between the plates. As described in Appendix A, this can easily be performed with our finite element model. However, because the 'superposition principle' holds in systems having a viscoelastic rheology, there are various ways to perform the computation, technically quicker, which provide exactly the same results (see Appendix A).

In this section, we will study precisely the dependence of the deformation field on the asthenosphere rheology, period of the cycle, locking depth and on the presence of a low viscosity wedge (LVW).

4.1. Maxwell rheology

The first results described here in Figs. 2 and 3 concern the most commonly used Maxwell viscoelastic rheology (cf. Appendix B) in the asthenosphere. The case of Figs. 2 and 3 has been obtained for a viscosity in the asthenosphere $\eta = 10^{19}$ Pa·s, with a period of the seismic cycle $T = 170$ years, a locking depth $h = 40$ km and without LVW. Fig. 2 depicts typical 'interseismic' (end of cycle) horizontal and vertical velocities as a function of distance to the trench, for both subducting (left part of the figure) and overriding plates (right part of the figure).

In order to have a more comprehensive view of the deformations during the seismic cycle – i.e. the coseismic, the postseismic and interseismic phases – the horizontal (Fig. 3a) and vertical displacements (Fig. 3b) as functions of time during the seismic cycle are shown at several distances from the trench (100 km, 250 km, 400 km, 700 km and 900 km). As mentioned above, the interseismic velocities plotted in Fig. 2 are in fact the slope at the end of the cycle of the displacement curves such as presented in Fig. 3. It is important to keep in mind that the velocities vary permanently through the seismic cycle and the velocities at the middle of the cycle are different from the velocities at the end of the cycle (interseismic velocities). This is especially true at large distances from the trench.

We will name here "near-field deformation" the part of the deformation occurring between 0 and 150 km from the trench, "middle-field deformation" the deformation between 150 km and 400 km from the trench and far-field the deformation which occurs further.

The most noticeable difference between elastic and viscoelastic models in Fig. 2a is that a significant part of the convergence velocity is not accommodated close to the trench but over a broad region, here reaching 2000 km. We will see in further sections that this distance depends upon the asthenosphere viscosity and upon the period of the seismic cycle.

The vertical interseismic velocities for elastic and viscoelastic models also show important differences (Fig. 2b): although similar amplitudes are observed in the near-field, the viscoelastic model shows a large subsidence at 400 km and uplift between 500 and 1000 km, whereas the elastic model shows no vertical motions in the far field. Note however, that, in the near-field, elastic and viscoelastic models yield very similar responses. Near-field data seem then inappropriate in the discussion of the mechanical properties of the asthenosphere. We will see that this stays true as long as the locking depth is smaller than the lithospheric thickness (Savage and Prescott, 1978).

¹ Where ρ is the density of the lithosphere, g the gravity and U_y the vertical displacement of the surface.

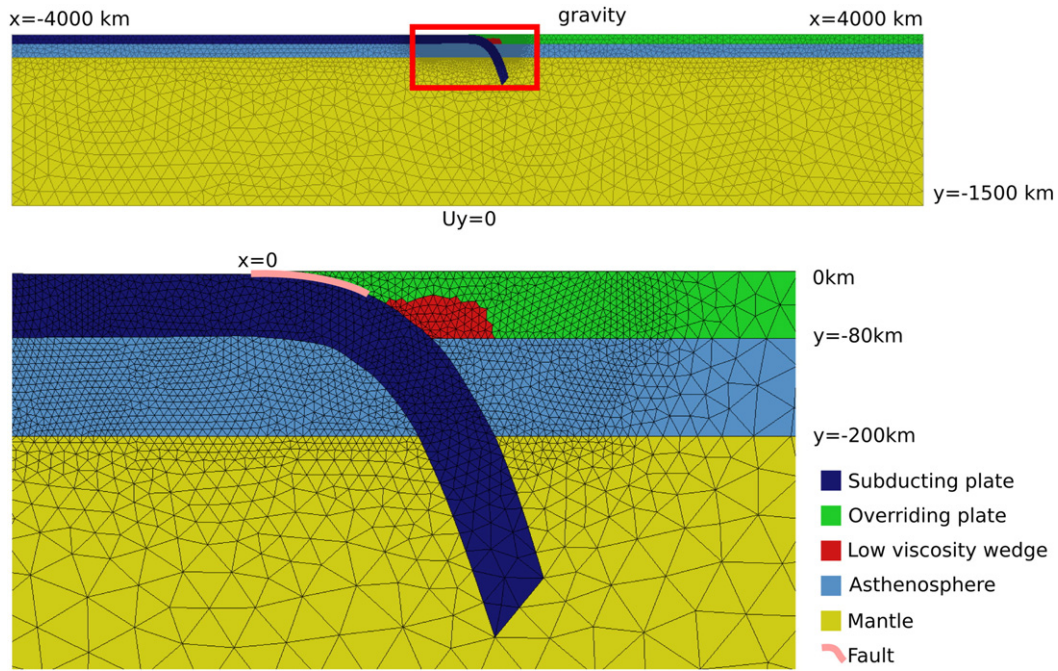


Fig. 1. Finite element model structure.

The interseismic viscoelastic vertical velocities compensate velocities of opposite sign during the first part of the cycle, i.e. uplift in the near-field and subsidence in the far-field during the postseismic phase (see Fig. 3b). This type of postseismic far-field subsidence is well documented in Thailand and is one of the arguments which convinced us that viscoelasticity was an essential ingredient of the seismic cycle. As shown in Fig. 3a, the large value, with respect to the elastic backslip case, of the horizontal interseismic velocities in the far field is just a consequence of strong postseismic phase in the same direction as the coseismic displacement, also well documented in Thailand.

4.2. Maxwell versus Burger rheology

In the present work we compare two different types of rheologies for the asthenosphere: Maxwell and Burger rheologies (see Appendix B). The analysis of postseismic data in South Asia is in favour of a Burger model with the following parameters: μ_1 is given by PREM, $\eta_1 = 3 \times 10^{19}$ Pa·s, $\mu_2 = \mu_1/3$ and $\eta_2 = 3 \times 10^{18}$ Pa·s.

Fig. 4 shows the comparison of the interseismic horizontal and vertical velocities for an elastic backslip model and five viscoelastic models. The two Burger models have a short-term viscosity equal to the long-term viscosity of one of the Maxwell models (see figure caption of Fig. 4). It should be noticed that the near-field horizontal responses of all those models are similar. The differences start to show at 200 km from the trench: the horizontal velocities in the mid- and far-field are attenuated with the Burger model compared to the Maxwell model but are larger than for the elastic model. However, the pattern of interseismic velocities as function of distance alone would not allow to discriminate between Burger versus Maxwell models as an increase in the asthenospheric viscosity can also affect the amplitude of the interseismic velocity for the Maxwell model.

The Maxwell model with $\eta = 10^{20}$ Pa·s gives results almost similar to the elastic backslip model: such high viscosities are not effective at the time scale of the seismic cycle (170 years in our case) and thus the material behaves almost elastically. Fig. 5 shows the predicted horizontal and vertical displacements as functions of time for the various models at 700 km from the trench. Since the first three models use the same 'short-term' viscosity (3×10^{18} Pa·s), the

postseismic response is similar for those models during the first 4 years. However, the Burger models saturate faster, and the interseismic signals of the various models differ strongly. If the

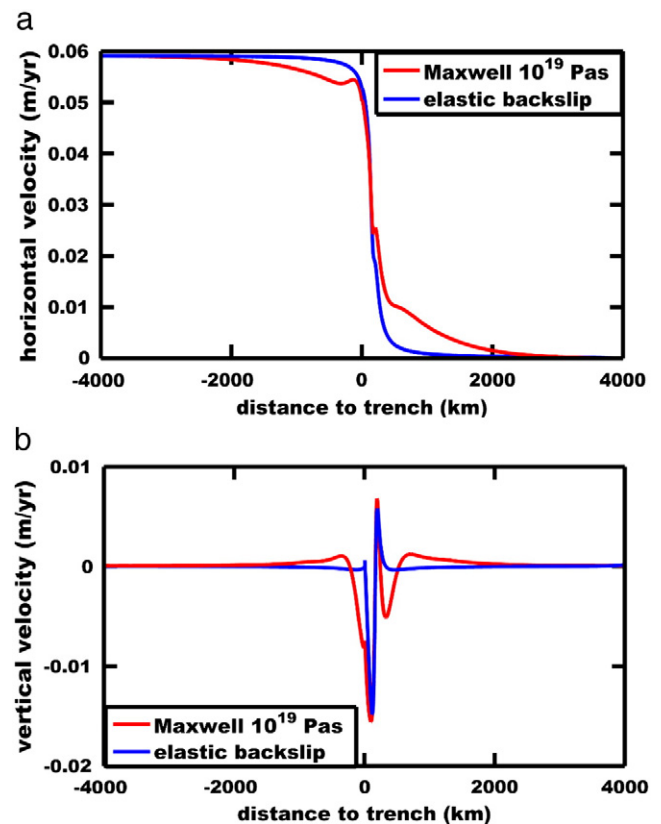


Fig. 2. Horizontal (a) and vertical (b) velocity in the overriding plate referential at the end of the cycle for the following case: Maxwell rheology in the asthenosphere with viscosity $\eta = 10^{19}$ Pa·s, period of the cycle $T = 170$ years, locking depth $h = 40$ km, amplitude of the coseismic slip 10 m and without LVW. The blue curve pictures the same quantities but for an elastic backslip model.

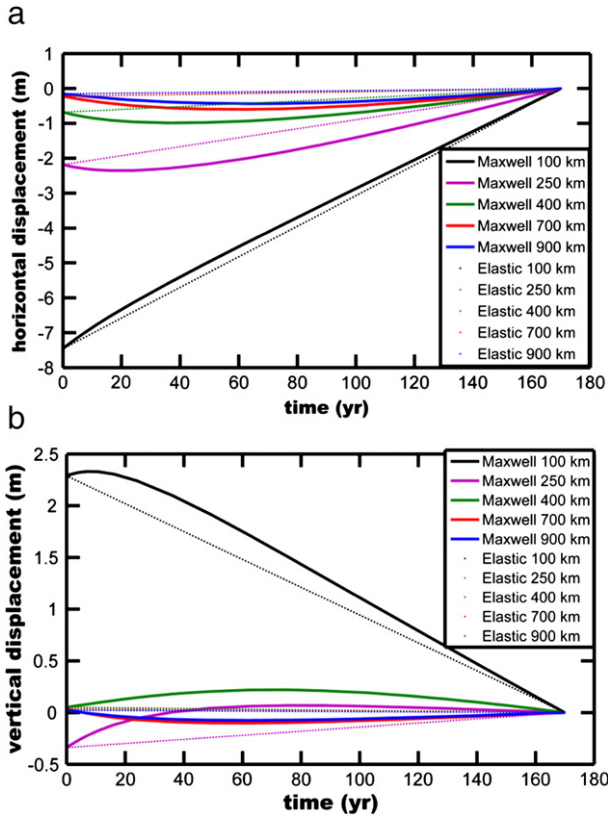


Fig. 3. Horizontal (a) and vertical (b) surface displacements on the overriding plate at various distances from the trench. The model parameters are the same as for Fig. 2. The displacements are plotted in the overriding plate referential.

overriding plate encounters no long-term deformation, the measured ratio postseismic over interseismic velocities should be able to indicate clearly whether Maxwell or Burger models are the most appropriate.

4.3. The period of the seismic cycle and the asthenospheric viscosity: two parameters influencing the amplitude of the far-field over near-field interseismic deformation

Depending upon the local geological context, both the typical time interval between large earthquakes (period of the seismic cycle in our simplified model) and the asthenospheric viscosity may be different from the values chosen here. How would it affect the interseismic velocities? While the red curve of Fig. 6 represents the interseismic velocities for our standard Burger case, the blue curve corresponds to a case with a coseismic slip of similar amplitude but a cycle period four times larger (the convergence velocity is then divided by 4). The black curve is the blue curve simply vertically dilated by a factor 4 (same convergence velocity as our standard Burger case but cycle period 4 times larger). Note that it corresponds then also to a ‘standard’ case either with mantle viscosities four times smaller. Indeed, because all the mechanical equations can also be put in a non-dimensional form where only the coefficient $\frac{\eta_{ref}}{T_{ref}}$ plays a role, lowering the viscosity or increasing the period leads to the same non-dimensional equations (η_{ref} and T_{ref} are here reference viscosity and time used to non-dimensionalise the equations (Thatcher and Rundle, 1979)). The smaller the viscosity (or the larger the period), the larger the distance over which the seismic cycle affects the deformations within the overriding and also the subducting plates.

Another quantity of interest is the ratio of interseismic plate convergence velocity measured over a short distance from the subduction fault (400 km) to the total (far-field) plate convergence

velocity. In our present model, the convergence averaged over a long period of time occurs over a very short distance, across the trench and there is no long-term intraplate deformation. It is however interesting to notice that an observer who would have only velocity measurements corresponding to the black curve and who would assume an ‘elastic backslip’ earthquake cycle (he would consider that the velocity difference between +400 and -400 km from the trench is the long-term velocity across the fault) would underestimate quite considerably the amount of long-term convergence across the subduction fault. The larger the period of the cycle or the smaller the viscosity, the larger the error. While we discuss in the present paper only the case of inverse subduction faults, the physics of this phenomenon would be the same for transcurrent faults, for example in Asia.

Although it contains some oversimplifications like the lack of elasticity in the sublithospheric mantle, the analytic Elsasser model (Elsasser, 1969; Bott and Dean, 1973; Melosh and Fleitout, 1982) enlightens several aspects of Fig. 6. This Elsasser model leads in particular to a diffusive equation with a diffusion coefficient $D = \frac{hH\mu}{\eta}$ i.e. to a length of penetration equal to $\sqrt{D \cdot T}$ where h and H are the thicknesses of the lithosphere and asthenosphere, μ the shear modulus, η the viscosity of the asthenosphere and T is the period of the seismic cycle.

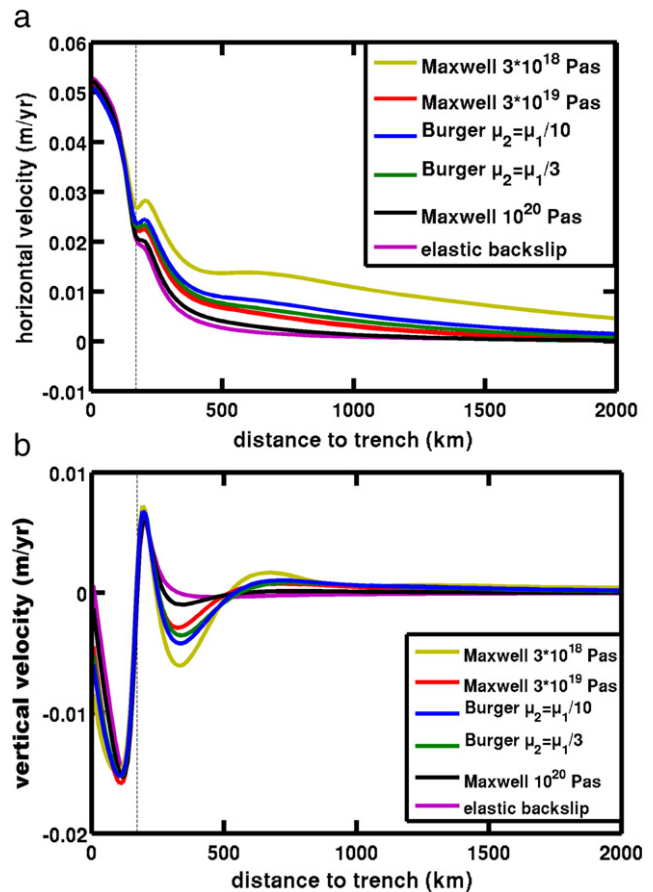


Fig. 4. Horizontal (a) and vertical (b) velocities at the end of the cycle for different rheologies: Maxwell rheology in the asthenosphere with a viscosity $\eta = 3 \times 10^{18}$ Pa·s, Maxwell rheology in the asthenosphere with a viscosity $\eta = 3 \times 10^{19}$ Pa·s, Burger rheology in the asthenosphere with $\mu_2 = \mu_1/10$, $\eta_1 = 3 \times 10^{19}$ Pa·s and $\eta_2 = 3 \times 10^{18}$ Pa·s, Burger rheology in the asthenosphere with $\mu_2 = \mu_1/3$, $\eta_1 = 3 \times 10^{19}$ Pa·s and $\eta_2 = 3 \times 10^{18}$ Pa·s, Maxwell rheology in the asthenosphere with the viscosity $\eta = 10^{20}$ Pa·s and elastic model. The locking depth for all the cases is $h = 40$ km, the coseismic slip 10 m, the period of the cycle $T = 170$ years and the models don't contain LVW.

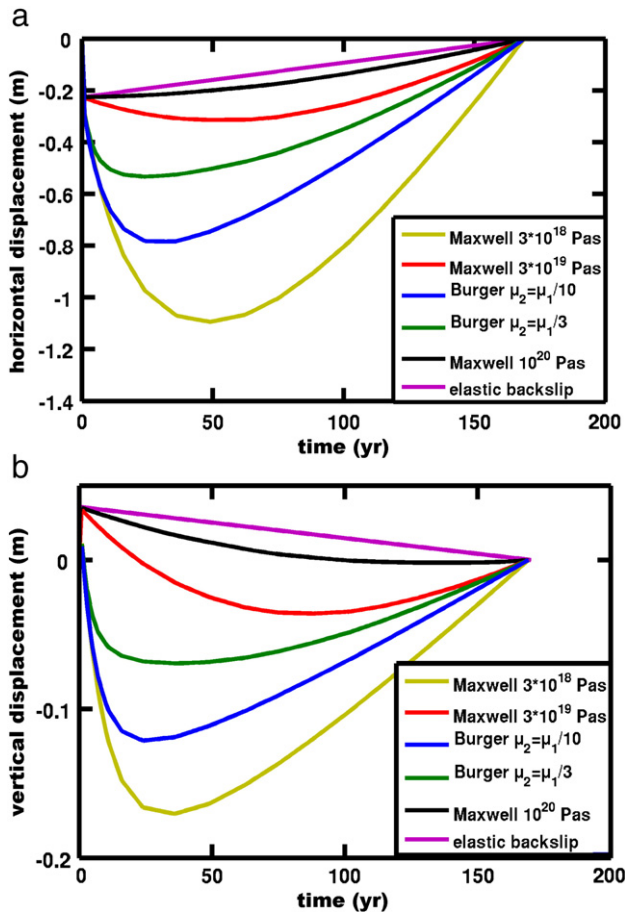


Fig. 5. Horizontal (a) and vertical (b) displacement at 700 km from the trench. The rheologies and the other parameters of the model are the same as for Fig. 4.

4.4. Effect of the locking depth

As shown in Fig. 4, the positive peak of vertical interseismic velocity is at the same distance from the trench for elastic models and for the viscoelastic models with a constant plate thickness. The position of the peak in vertical interseismic velocity and its maximum value depend on the locking depth of the model. This is well known for elastic backslip models. It is also true for viscoelastic models which involve an overriding plate of constant thickness, as shown in Fig. 7. This figure depicts the predicted interseismic velocity field for various locking depths. The geometry of the fault is the same for all models. This very good correlation between the site where the vertical motion goes from negative to positive and the end of the locking zone has been very extensively used to determine the locking depth of various subduction zones (Simoes et al., 2004).

As already noticed by Savage and Prescott (1978) the locking depth over thickness of the elastic lithosphere is the parameter which determines whether the interseismic velocity presents a sharp gradient in the near-field or whether it decreases progressively over a long distance range. To illustrate this point, we have chosen a model with an elastic lithosphere of thickness 38 km and a viscosity stratification similar to that of previous models. Fig. 8 compares cases with locking depths 37 km and 18 km. In the first case, the velocity decreases progressively over a very broad zone and there are no sharp near-field gradients of velocity. Elastic and viscoelastic solutions differ even in the near-field. A similar very broad velocity gradient can be seen on the curve for a locking depth of 60 km of Fig. 7. However, it must be noted that it is not the absolute value of the locking depth which matters but the ratio of the locking depth to the thickness of the elastic lithosphere. Indeed the case with

locking depth 40 km from Fig. 7 presents a relatively sharp near-field velocity gradient while the locking depth is there deeper than for the cases of Fig. 8. On the other hand, when the locking depth is much shallower than the base of the elastic lithosphere (case with locking depth 18 km in Fig. 8), more than 70% of the velocity jump between the two plates occurs within 200 km from the trench (blue curve in Fig. 8) and the near-field displacements for elastic and viscoelastic solutions are very similar. Fig. 8 shows then that if the ratio locking depth over thickness of the continental elastic layer is significantly smaller than 1, one obtains a sharp gradient of velocity in the near-field. Ali and Freed (2010) attributed the sharp gradient they observe in interseismic profiles in Alaska to a high asthenospheric viscosity leading to an elastic backslip model. We claim here that such a sharp gradient could as well be compatible with a low viscosity asthenosphere as long as the thickness of the elastic plate is significantly larger than the locking depth.

As has been discussed in Section 4.3, the mantle viscosity (or rather the ratio mantle viscosity over cycle period) affects then the amplitude of the velocity jump in the near-field and also the width of the far-field zone over which the velocity slowly decreases.

4.5. Low viscosity wedge

In the previous sections, the overriding plate was assumed to have a uniform thickness. However, in the neighbourhood of a subduction zone, this seems rather unlikely: seismic and petrologic data have put

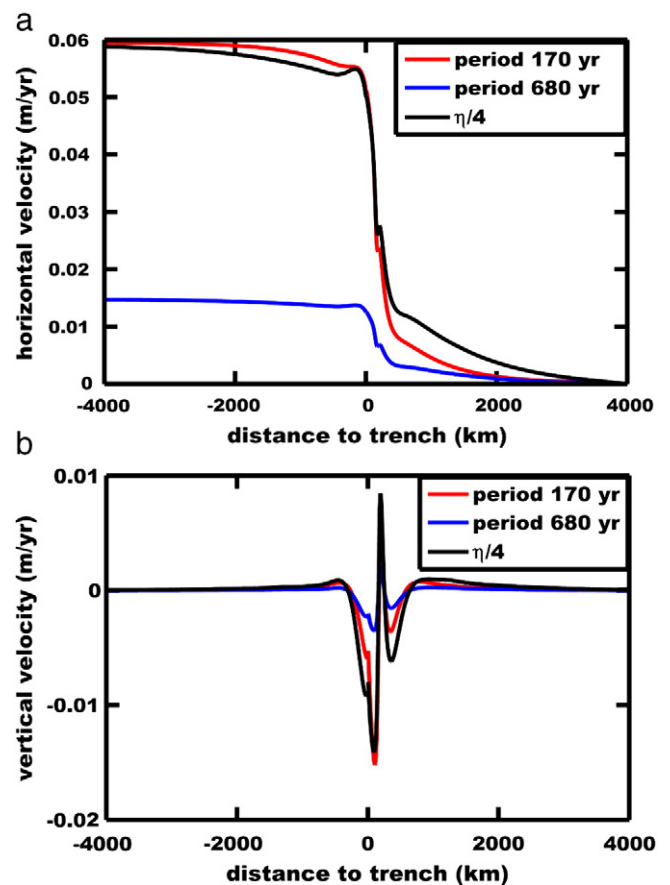


Fig. 6. Horizontal (a) and vertical (b) velocities at the end of the cycle for different periods of the seismic cycle: 170 yr (standard period) and 680 yr (4 times larger). The locking depth for all the cases is $h = 40$ km, there is no LVW and the coseismic slip is 10 m. For the red and blue curves, the model has a Burger rheology in the asthenosphere with $\mu_2 = \mu_1/3$, $\eta_1 = 3 \times 10^{19}$ Pa·s and $\eta_2 = 3 \times 10^{18}$ Pa·s. η_1 and η_2 have been divided by 4 for the black curve. The velocity on the black curve is exactly equal to that of the blue curve multiplied by 4.

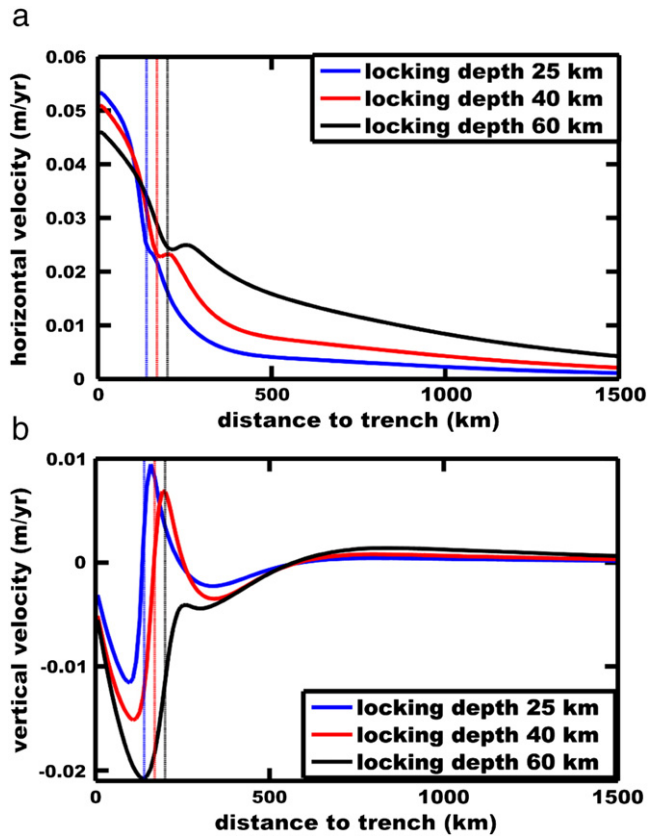


Fig. 7. Horizontal (a) and vertical (b) velocities at the end of the cycle for different locking depths: 25 km, 40 km and 60 km. The model has a Burger rheology in the asthenosphere with $\mu_2 = \mu_1/3$, $\eta_1 = 3 \times 10^{19}$ Pa·s and $\eta_2 = 3 \times 10^{18}$ Pa·s. There is no LVW, the period of the cycle $T = 170$ years and the coseismic slip is 10 m. The vertical dashed lines mark the limit of the locked zone.

forward the idea of a “low viscosity wedge”, in the corner at the base of the lithosphere between the island arc and the subducting plate. This low viscosity wedge (LVW) is indeed thought to have a very low viscosity as it is assumed to be partly composed of serpentine which is very ductile (Peacock and Hyndman, 1999). Below the island arcs, the lithosphere is also very thin as suggested by heat-flow and seismic tomography data.

In the present model, we keep the shape and mechanical properties of this LVW very simple, with the same rheology for the hot zone below the island arc and for the serpentinized zone. In more elaborate models, it might be useful to include a particular rheology for the zone of partial serpentinization. If the non-serpentinized mantle stays elastic, this heterogeneous zone may behave like a Kelvin–Voigt viscoelastic solid, with transient creep corresponding to viscous relaxation in the ‘pockets’ of serpentine. However, the resisting zones of non-serpentinized mantle seem to break during the seismic cycle, giving rise to earthquakes like the Miyagi earthquake (Yamamoto et al., 2006), and thus finally they may not bear the stresses generated during the seismic cycle. In our view, what we model here in a simplified way as a LVW includes this zone of partial serpentinization and then it may be present at depths somewhat shallower than the maximum depth of earthquakes on the subduction interface. The early phase of many giant earthquakes may occur in this intermediate heterogeneous-viscous–brittle layer and its deformation during the seismic cycle deserves further attention.

Fig. 9 compares the interseismic velocities for the cases without a LVW and with three differently sized LVW. As one can see, the peak in vertical velocity for the cases with LVW is situated further away from the trench: the broader the low viscosity wedge, the further away the

peak. The LVW also induces larger horizontal interseismic velocity in the close and middle field. These larger interseismic velocities are the consequence of larger postseismic velocities.

Fig. 9 left shows the so-called “non-touching case”, where the fault is disjoint from the LVW, whereas the curves on the right are for “touching case”, where the fault penetrates 10 km deep into the LVW. The touching case shows larger vertical and horizontal velocities in the near-field; the non-touching case is perhaps physically more realistic and has our preference.

4.6. Our preferred model

To conclude this discussion of various model ingredients, our preferred model based on the analysis of Sumatra postseismic deformations, involves a low viscosity wedge (viscosity $\eta = 0.5 \times 10^{19}$ Pa·s) and a Burger viscoelastic rheology where μ_1 is given by PREM, $\eta_1 = 3 \times 10^{19}$ Pa·s, $\mu_2 = \mu_1/3$ and $\eta_2 = 3 \times 10^{18}$ Pa·s. Fig. 10 presents the horizontal and vertical displacements through the whole seismic cycle for this particular set of parameters. This figure should be compared to Fig. 3. Both figures are rather similar; however the Burger rheology induces a shorter postseismic phase at large distances. The low viscosity wedge induces a huge difference in the middle-field.

5. Comparison with previously proposed models of interseismic motion

We will now compare the results obtained with a viscoelastic model (with our preferred set of parameters) with previously proposed models for computing the interseismic velocities: an elastic backslip model and a viscoelastic model where lateral viscosity variations are neglected.

5.1. Elastic backslip

The analytic formulation of dislocation model obtained by Savage (1983) is simple and consequently has been used very often. The case involving a uniform elastic half space (Okada, 1985) has been particularly popular. Fig. 11 compares the velocities predicted for elastic models and those inferred from viscoelastic models without low viscosity wedge (for the difference with the case with a low viscosity wedge, refer to Fig. 9).

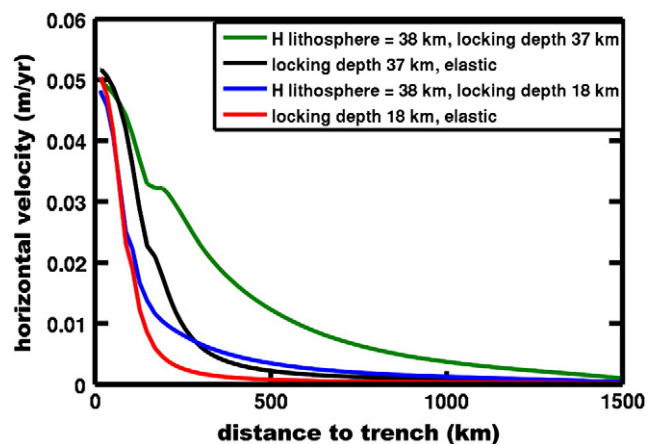


Fig. 8. Horizontal velocity at the end of the seismic cycle as a function of the distance to the trench for the model with a 38 km thick lithosphere, for elastic and viscoelastic cases with our standard parameters. There is no LVW. The locking depth is 37 km (green and black lines) and 18 km (blue and red lines).

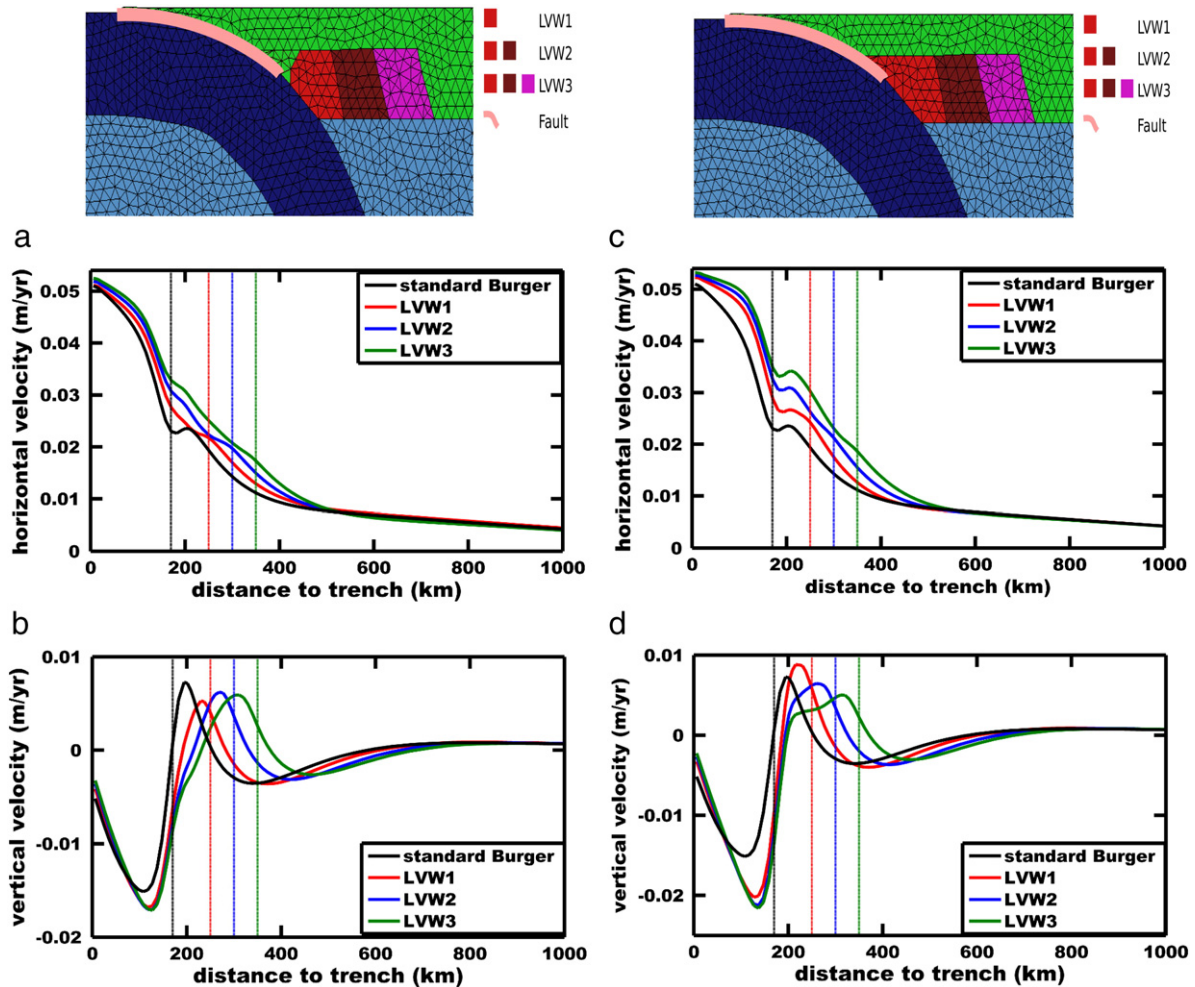


Fig. 9. Horizontal (a, c) and vertical (b, d) velocities at the end of the cycle for the standard case and the cases with LVW and the structure of LVW. The standard case is has a Burger rheology in the asthenosphere with $\mu_2 = \mu_1/3$, $\eta_1 = 3 \times 10^{19}$ Pa·s and $\eta_2 = 3 \times 10^{18}$ Pa·s, without LVW, the period of the cycle $T = 170$ years. The cases with LVW have a Maxwell rheology in the LVW with a viscosity $\eta = 0.5 \times 10^{19}$ Pa·s and the same rheology in the asthenosphere as the standard case. The black dashed line marks the limit of the locked zone. The colour dashed lines indicate the eastern extent of the LVW (LVW1 250 km (red line), LVW2 300 km (blue line) and LVW3 350 km (green line)). Locking depth is $h = 40$ km for all the cases. Figures a and b – “non-touching” case, and c and d – “touching” case.

It should be noted that elastic models with a realistic depth dependence of the elastic parameters yield interseismic velocities rather different from models involving a uniform elastic half-space. For example, at large distances, the horizontal velocities differ by a factor larger than 2. The elastic backslip interseismic velocity just corresponds to the coseismic divided by the period of the seismic cycle (see Fig. 3). The difference between the two elastic models is a perfect illustration of the fact that the response to a dislocation is very different for a uniform elastic half-space and for a more realistic distribution of elastic properties: even for the analysis of the observed coseismic displacements in terms of slip on the fault plane, we believe that it is very important to take into account a realistic depth dependence of the elastic parameters.

On the other hand, we tested the effect of lateral variations of elastic coefficients linked to a cold slab or to a continental crust thicker than the oceanic crust and we found a negligible impact.

In the region between 100 and 170 km from the trench, the responses of the viscoelastic model and of the two elastic models are rather similar. However, the models differ strongly close to the trench and in the middle and far-field where the viscoelastic model is associated with much larger interseismic velocities. The difference between elastic and viscoelastic models becomes large in the region around 200 km from the trench when the low viscosity wedge is taken into account.

5.2. No slab

Viscoelastic models often assume for simplicity that there is no slab penetrating in the mantle, e.g. only assume depth-dependent variations of the viscosity (layered layout). This assumption allows the use of spectral techniques to compute the response of the model. However, the presence of a penetrating slab induces a stiff zone at asthenospheric depths. The red curve of Fig. 11 shows the horizontal and vertical velocities obtained with the layered assumption while the green curve represents exactly the same case but with an elastic subducting plate. The velocities for these two cases are very different, almost as different as the elastic and viscoelastic cases in the close and middle field. So we deem important to include all known sources of lateral viscosity variations when studying either the interseismic or the postseismic signals.

6. Some applications of the viscoelastic model

6.1. Far-field interseismic velocity in Sundaland

The deformation in Sundaland is particularly interesting as there has been GPS measurements in Indonesia, Malaysia and Thailand both before (Bock et al., 2003; Michel et al., 2001; Simons et al., 2007) and after the great Aceh subduction earthquake on December

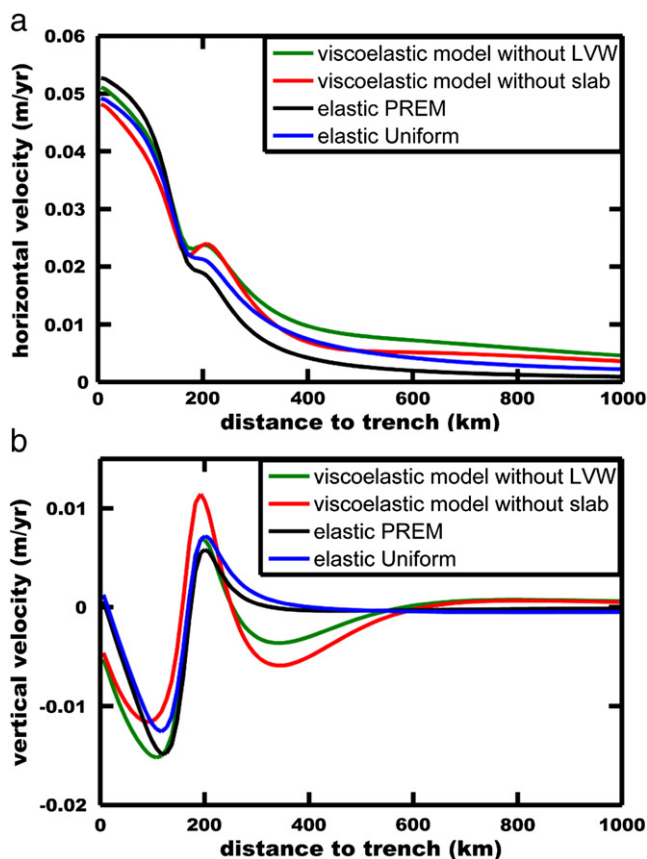
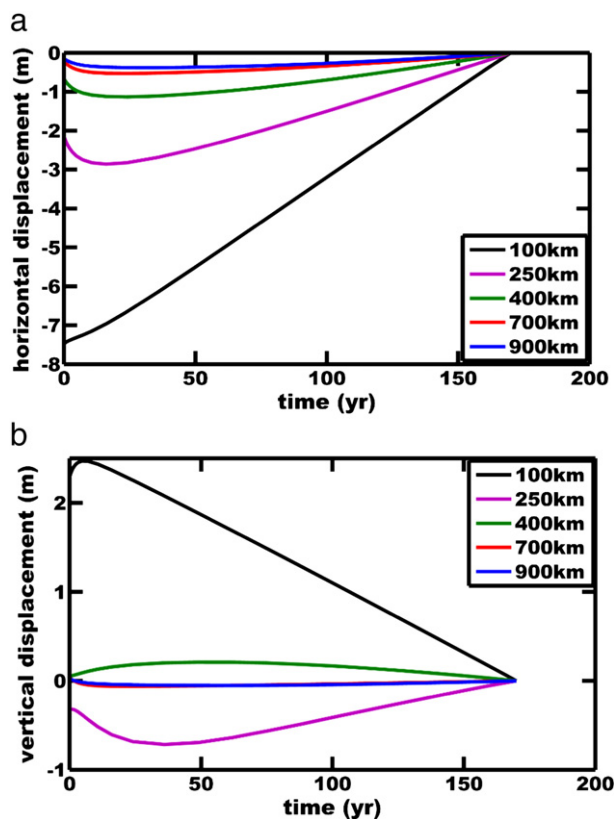


Fig. 10. Horizontal (a) and vertical (b) surface displacements as a function of time for our preferred model at various distances from the trench in the referential of the over-riding plate. The model has the standard Burger rheology in the asthenosphere (see Fig. 7). The LVW has a viscosity $\eta = 0.5 \times 10^{19}$ Pa·s, the locking depth is $h = 40$ km and the period of the cycle is $T = 170$ years.

Fig. 11. Comparison between horizontal (a) and vertical (b) velocities obtained for elastic backslip models and viscoelastic models. The viscoelastic models have the standard Burger rheology in the asthenosphere (see Fig. 7). The models don't contain a LVW and the red curve corresponds to the case where the lateral viscosity variations linked to the presence of the slab deeper than 80 km have been neglected. The period of the cycle is $T = 170$ years and the locking depth is $h = 40$ km.

26th 2004. The postseismic deformation in Thailand is huge (Satirapod et al., 2012) and this mere assessment suggests that there must be a sizable signal linked to the seismic cycle in the pre-earthquake signal (simply because the interseismic must compensate for the co- and postseismic deformations). Using the vertical subsidence, we have been able to show that a large part of the postseismic signal is a consequence of viscoelastic relaxation in the asthenosphere.

Is the viscoelastic model which fits the postseismic deformations also consistent with the interseismic deformations? Fig. 12a illustrates the interseismic velocity field of Sumatra and adjacent areas relative to the South China reference frame. We did not plot here the error ellipses associated with the velocities deduced from GPS campaigns, corresponding to σ of typically 0.5 to 1 mm/yr. Local hydrological or anthropic perturbations may induce larger shifts of the geodetic points.

Previous studies by Bock et al. (2003) and Simons et al. (2007) have interpreted this interseismic signal by introducing a Sunda block. The rotation pole and velocity of this Sunda block were determined by looking for the best fit to pre-earthquake velocities measured in Malaysia and Thailand. According to the pre-earthquake velocities, this Sunda block encounters a slight north-south compression and moves northward with respect to South-China. This interpretation is indeed the correct one if the elastic backslip seismic cycle model holds as the interseismic motion in the far-field predicted by this model is negligible. However, as mentioned above, the mere observation of a strong postseismic signal in the far-field indicates that there should have been also a sizable interseismic signal.

A full 3D model, also including the Philippine subduction zone and the Sumatra fault system is necessary to model adequately the

interseismic velocity in the Sunda area. To check in a preliminary way whether the interseismic velocities predicted by our model could be responsible for the deformation observed in the Sunda area, we have plotted in Fig. 12b the north-south component of the velocity as a function of distance to the trench, and compared these measures with the results from our 2D model. The fit is rather good if one takes into account that highly and poorly coupled segments are all mixed and introduce dispersion in the short distance points. In the far-field, there is also the influence of the 'low coupling' Java segment and of Philippine subductions, not taken into account in our current 2D model. Although we do not pretend to model the interseismic velocities in the Sunda area with our 2D model, Fig. 12b strongly suggests that at least part of the internal deformation and velocity of the Sunda block with respect to South-China are in fact transient effects linked to the seismic cycle. The role of the Sumatra fault in accommodating the change of direction between the north-east, south-west coseismic and postseismic phase and the north-south interseismic phase remains to be clarified through a 3D study.

In a more general way, elastic backslip and viscoelastic models may give relatively similar deformations in the near-field as long as the locking depth is shallower than the elastic plate thickness. This explains the success of elastic backslip models. As elastic backslip does not induce sizable far-field interseismic signal, the far-field observed deformations have been very often associated with long-term intraplate or block-plate deformations. An important point of the present study is to claim that transient interseismic deformations

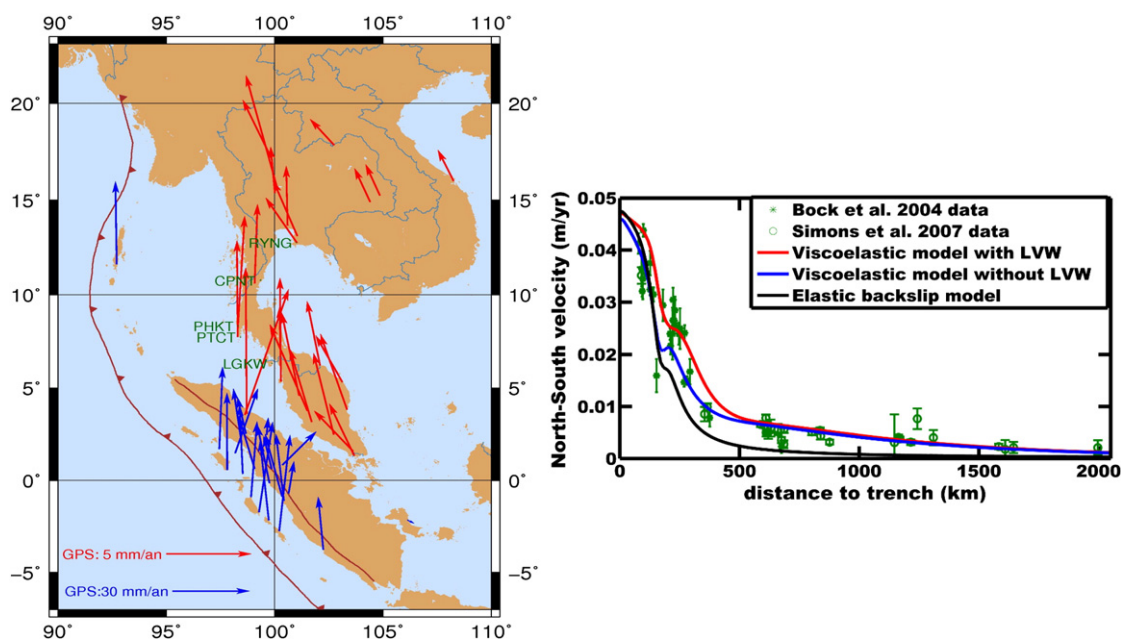


Fig. 12. Interseismic velocity field of Sumatra and adjacent areas relative to estimated South China reference frame (a) and the prediction of viscoelastic and elastic models. The viscoelastic models correspond to the standard case (Fig. 7). The viscosity in the LVW is $\eta = 0.5 \times 10^{19}$ Pa·s.

can perturb the velocity field recently measured by GPS at large distances from known faults and induce intraplate deformations which will be reversed during other phases of the seismic cycle.

6.2. Horizontal and vertical velocities in northern Honshu before the Tohoku earthquake

In the case of Tohoku, the peak in interseismic vertical velocity is in the western part of the district and an elastic backslip model would then imply strong coupling down to a depth of at least 100 km, which is unrealistic. This was first noticed in the classical paper of Savage (1983) who concluded that “this dilemma is unsolved”. There is moreover a strong E–W compression of the whole district (Mazzotti et al., 2000).

In Fig. 13, we have plotted as function of distance to the trench the horizontal and vertical velocities between 2001 and 2010 taken directly from the GSI site² (we only have the absolute value of the velocity for these points) and from the JPL web site.³ We took the data between 37° and 41° in latitude and eliminated stations at less than 70 km from an earthquake of magnitude larger than 6.5 for the GSI site stations. We also checked the time series and eliminated stations visibly perturbed by a local earthquake for the JPL stations. Some noise may remain, especially noise of climatic or anthropic origin in the vertical data. However, most of the datapoints confirm the gradient in vertical velocity from east to west noticed by Savage (1983), with uplift rather far away from the trench. The horizontal velocities show a very clear E–W trend, confirming a strong interseismic compression of northern Honshu. These velocities have been plotted in an Amurian plate referential, where the velocity of the permanent Changchun GPS station is assumed to be zero.

While an elastic backslip model would imply a coupling down to very large depths below the volcanic arc, our model incorporating a low viscosity wedge is able to explain the observed pattern of both horizontal and vertical deformations through Honshu, with moderate coupling depths. To model these deformations, we used a new mesh respecting the shape of the Japan subduction interface such as given on the USGS

website.⁴ The geometry of this interface is close to geometries proposed by Uchida et al. (2010) or Miura et al. (2005).

Although (partly because of the noise on the data), we are presently unable to determine unambiguously the locking depth and the shape of the low viscosity wedge (both blue and red curves in Fig. 13 fit the data), we definitely think that the presence of a low viscosity wedge is the way to reconcile the deformation in northern Honshu with a moderate coupling depth. Note that the lithosphere below central Japan is indeed very thin as indicated by heat-flow data (Tanaka et al., 2004) and that partial heterogeneous serpentinization is present up to rather shallow depths (Yamamoto et al., 2006).

The interpretation of the far-field horizontal velocities definitely requires 3D modelling, involving the subduction zones and tectonic features over a rather broad zone of eastern Asia (Apel et al., 2006; Jin et al., 2007), also adding long-term tectonic compression through the Japan Sea. We will simply mention that some of the previously proposed Okhotsk–Amurian plate convergence velocity might have been strongly overestimated as, in our view, the GPS datapoints on the west coast of Honshu had before Tohoku earthquake an eastward velocity component corresponding to an interseismic signal. Our models would also predict that there was elastic internal compression further within the Amurian plate at rates of a few mm/yr: the eastward velocity of the Changchun station was indeed some 3 mm/yr larger than the velocity at Vladivostok before Tohoku earthquake (Heki et al., 1999; Shestakov et al., 2010), in good agreement with this prediction. The present study suggests that in order to relate the long-term velocity of the Amurian plate to GPS velocity measurements, one should take into account perturbations linked to the seismic cycle of the Japan Trench Subduction and also of the Japan sea convergence zone. As mentioned in the next section, 2D models overestimate the displacements at distances from the trench larger than the width of the coupled segment. So we will not use Fig. 13 to provide quantitative estimates of the convergence rate between western Japan and the East coast of Asia which might be linked to the seismic cycle.

² http://mekira.gsi.go.jp/project/f3_10_5/en/index.html.

³ <http://sideshow.jpl.nasa.gov/mbh/series.html>.

⁴ <http://earthquake.usgs.gov/research/data/slab/>.

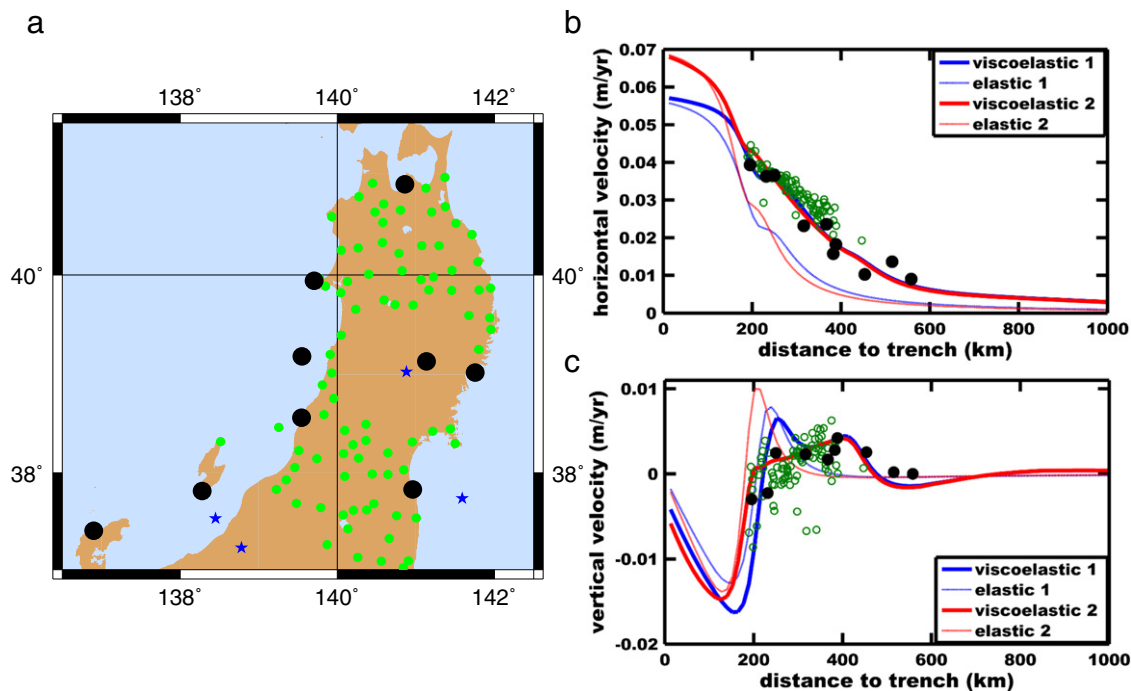


Fig. 13. GPS stations which provide the East and vertical velocities before Tohoku earthquake (a) and the prediction of viscoelastic models (b, c). The models correspond to the standard case. The viscosity in the LVW is $\eta = 0.5 \times 10^{19}$ Pa·s. The first model has a locking depth $h = 44$ km and a LVW “touching” the seismogenic zone. The second model has a locking depth $h = 36$ km and the LVW “doesn’t touch” the slip zone. The shape and position of the LVW is the same for the 2 models. The computation has been performed on a new mesh with a realistic geometry of the subduction interface corresponding to the geometry of the Japanese subduction (stretched horizontally in comparison to the standard case).

7. 3D Finite element modelling

All the above models are 2D models while, in the real Earth, the faults always have a finite lateral extent. A real subduction zone is usually made of various segments with different characteristic earthquake periodicity, coupling depth and geometry. It is then important to discuss in what sense the 2D results can be applied to a finite width fault segment. The contribution from each segment can be added afterwards. As any elliptical type of equation, the mechanical equations are expected to yield a geometrical attenuation with both the co- and postseismic signals (and as consequence the signal during the whole cycle) smaller for a segment of limited width compared to a 2D situation. What we want to test here is whether this geometrical attenuation affects the main conclusions obtained in 2D. We consider a portion of spherical shell from the core–mantle boundary to the Earth’s surface, from 5°N to 65°N in latitude and over 95° in longitude. The geometrical model is presented in Fig. 14 (this region is in fact centred over Japan, but it could be anywhere else on Earth: in the present section, we are simply interested in testing the 2D approximation). To model the earthquake cycle in 3D case, we use the same method as in 2D (Appendix A, the viscoelastic backslip’ or superposition of N individual earthquakes’ methods are particularly convenient). In order to examine the relationship between the predictions of 3D and 2D models, we consider displacements at points over a cross line roughly perpendicular to the trench in the middle of the segment (Fig. 15, red points) and also a side point (blue point in Fig. 15).

In order to test the impact of the lateral extent of the subduction segment we consider 3 cases (Fig. 15) – 1. slip on the whole subduction segment for 3D model (purple belt in Fig. 15); 2. slip on the central part of the subduction segment (green belt on Fig. 15); and 3. 2D model. To compare 2D and 3D models we plot the velocities 2 years after the earthquake as functions of the distance to the trench (Fig. 16a). This figure shows that the velocities 2 years after the earthquake, are as expected, larger for the 2D model (as a 2D model implies an infinite width of the subduction interface), then larger

for the wider subduction segment than for the narrower one. Fig. 16b shows the velocities 2 years after the earthquake divided by the coseismic displacement as a function of distance to the trench. As one can see, this ratio remains almost the same from 2D to 3D model.

To compare the seismic cycle for the 3D and 2D models we choose two points in the 3D model: a black point on the red line which we call “central point” and a blue point (“side point”) both situated at 700 km from the trench. For these two points we plot (Fig. 17) the amplitude of the horizontal displacement during the seismic cycle, normalised by the amplitude of the horizontal coseismic displacement. The same normalisation is applied to the 2D model (red curve).

Again, the three curves are rather similar. Note however that for the side point, the postseismic velocity in the years following the earthquake is not exactly in the same direction as the co- and interseismic velocities (Fig. 15). The early postseismic has a larger component parallel to the trench. One cannot of course compute accurately the 3D pattern of deformation simply from coseismic displacement and a 2D viscoelastic model. Qualitatively, however, all the conclusions from our previous sections involving a 2D model are expected to apply in 3D (effect of Burger rheology, of LVW of viscous slab at depth) and quantitatively, rather good estimates are obtained if one renormalizes the results by the amplitude of the horizontal coseismic displacement.

The results from Figs. 16b and 17 also explain very well one of the observations we made on our data in SE Asia: all our curves of horizontal postseismic displacement in the far-field (600 km–1500 km from the trench), non-dimensionalized by the coseismic displacement seem to be similar. It can indeed be deduced from Figs. 16b and 17 that at these distances, the normalised displacements are expected to be rather independent from the distance to the trench and from the position of the considered point (more or less “central”).

8. Conclusion and discussion

One of the first purposes of the analysis of interseismic deformation is to improve our understanding of stress accumulation process

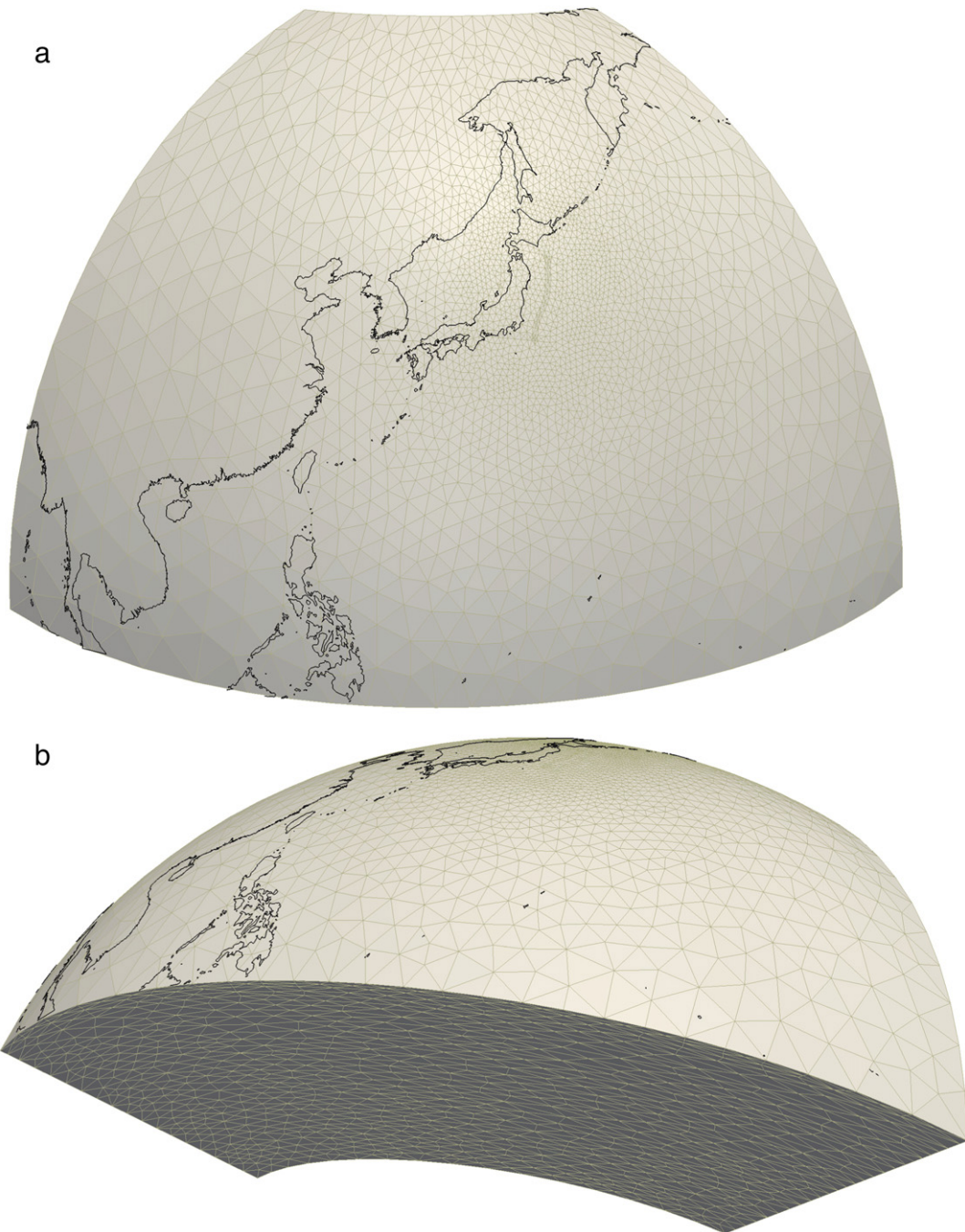


Fig. 14. 3D Finite element structure used to study the effect of 3D geometry, represented as a portion of a spherical shell from the core–mantle boundary to the earth's surface, from 5°N to 65°N in latitude and over 95° in longitude.

before large earthquakes, leading in turn to better insights on the seismic hazard associated with a given subduction segment.

The conclusions of the present study strongly disagree with the general belief that the interseismic signals predicted by viscoelastic and elastic models are very similar: in the near-field and middle-field (<300 km), when the locking depth is shallower than the thickness of the lithosphere, viscoelastic models without low viscosity wedge and backslip elastic models yield indeed rather similar deformations although the amplitudes of the predicted velocity jump across the near-field zone can be considerably reduced in the case of a viscoelastic rheology. However, the presence of a low viscosity wedge in the viscoelastic models shifts continentward the position of the peak in vertical velocity; in some cases it may even induce

two peaks. It also shifts continentward the region of strong horizontal compression (or strong horizontal velocity gradient).

In the far-field, the difference between elastic and viscoelastic models is even more noticeable: for example, at 1000 km from the trench, for rheological properties able to provide a good fit to the Aceh earthquake postseismic signal, we predict a 5 mm/yr perturbation of the horizontal velocity in the overriding plate due to the interseismic signal, while it reaches only 1 mm/yr in the elastic case. Using elastic backslip models to map the 'coupling' over a subduction interface might thus be misleading, even if only near and middle-field data are used, leading in particular to an overestimated coupling depth.

Is there a way to compute interseismic velocities simpler than the finite element models mimicking the whole seismic cycle proposed

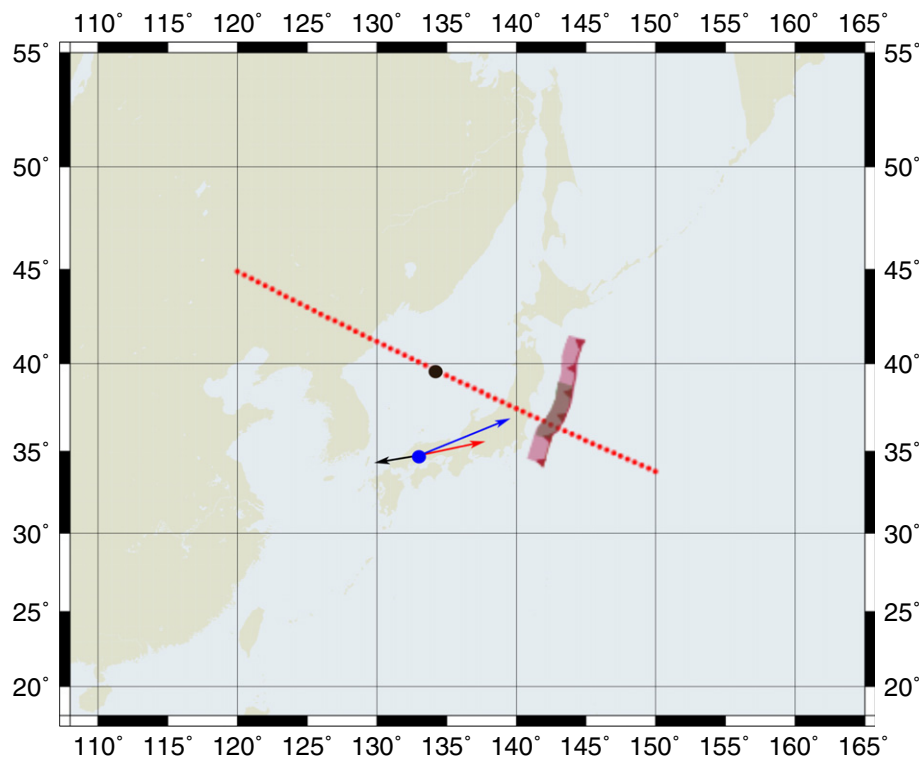


Fig. 15. The position of the coupled zones. We will consider periodic earthquakes either on the whole segment (purple belt) or on a narrower segment (green belt). To compare the results of 3D model with 2D model we use the cross-section of 3D model perpendicular to the trench – red points (Fig. 16). To compare the results for the whole seismic cycle from 3D and 2D model (Fig. 17), we use “central point” (black point) and “side point” (blue point) which are located 700 km away from the trench. Red, blue and black arrows correspond respectively to coseismic displacement, postseismic velocity (at 2 years) and interseismic velocity. The absolute values are 12.83 cm for coseismic displacement, 1.88 cm/yr for postseismic velocity and 0.89 cm/yr for interseismic velocity.

here? We have shown that taking into account the lateral viscosity variations associated with the slab at depth and with the LVW is important. Models based on spectral methods which cannot include lateral viscosity variations thus do not seem appropriate. Interseismic velocities are intrinsically linked to the typical time-scale of the seismic cycle and therefore to the past regional earthquake history. Not modelling the whole cycle but using viscoelastic ‘steady-state’ backslip (Hu et al., 2004) also provides inappropriate interseismic velocities.

The output from the present paper has already been used to predict when the postseismic subsidence will stop in Thailand (Satirapod et al., 2012) and also when to expect a peak in extensional stress, potentially generating intraplate earthquakes, in the Indian plate, a few hundred of km away from the trench (Delescluse et al., 2012). Time-scales of the order of 10 yrs were predicted for both phenomena.

Another implication of the present study concerns the very understanding of intraplate deformation. In tectonic areas, the GPS deformation fields usually show large deformation gradients at short distances from major faults, and between these faults broad regions deforming more or less continuously with low strain rates. As already pointed by Hetland and Hager (2004), such a pattern can be interpreted in two different ways:

- The elastic backslip interseismic pattern may account for the region of strong deformation gradient close to the fault and a permanent plastic slow deformation of the whole lithosphere may be responsible for the slow background deformation.
- As shown by Fig. 12b, if the asthenosphere or the lower crust has a sufficiently low viscosity, this pattern can also be interpreted as the consequence of interseismic motion without long-term plastic deformation of the lithosphere except on faults: this is in fact what has been proposed here in Section 6 where we claimed that the

observed pre-2004 internal compression of the Sunda block and its north–south velocity with respect to South-China might be mainly due to elastic deformations of the lithosphere at the end of the seismic cycle.

The same reasoning would apply as well to transcurrent faults in Asia. As shown in Fig. 6, for long seismic cycles or for low viscosities in the asthenosphere or lower crust, the apparent velocity across the fault computed from the velocity jump across the high deformation gradient area might be much smaller than the real long-term velocity across the fault. Depending upon whether one chooses to interpret the present-day intraplate deformations patterns obtained from GPS measurements with an elastic or a viscoelastic view of the asthenosphere, the estimated amount of long term discrete (on faults) versus continuous deformation will be very different.

Deciphering in the future GPS velocity fields what is due to real continuous plastic intraplate deformation from what is the consequence of elastic deformation within the seismic cycle will be one of the tasks of 21st century studies. The coupling between these two types of deformation will certainly be a fascinating field to explore.

Appendix A. Viscoelastic models of interseismic motion

We show here that there are several equivalent methods for computing the deformations during the seismic cycle. The “realistic” model is schematically represented on Fig. A1a, b. The model features an asthenosphere, a low viscosity wedge (LVW), plate velocities imposed in the far-field and periodic earthquakes on the upper part of the subduction interface. In order to conserve the volume, we impose on the lateral boundaries a return flow (small arrows) to compensate the inward flow of matter imposed by the plate motion (large arrows).

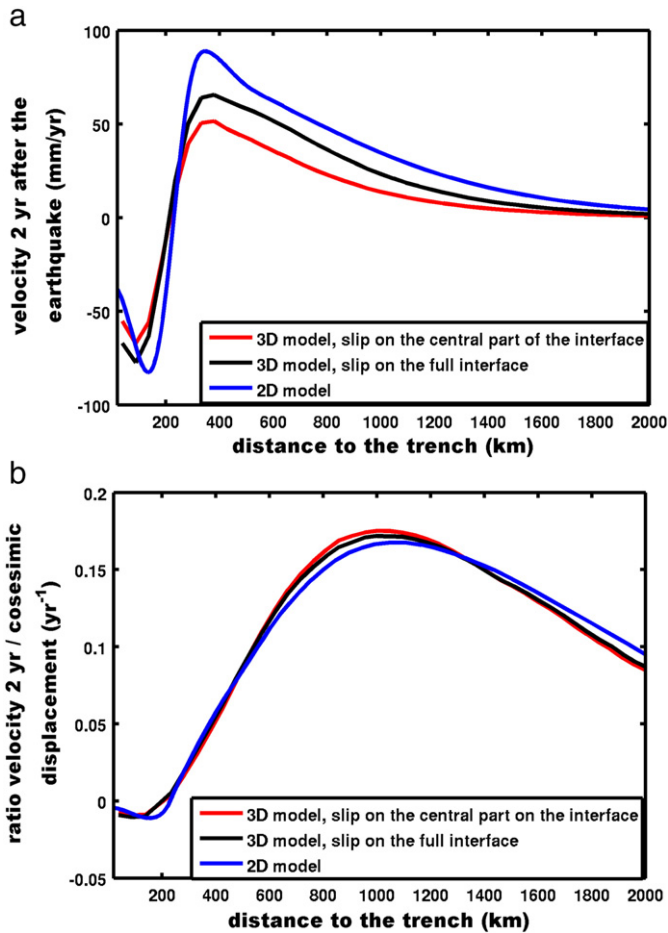


Fig. 16. Velocity 2 years after the earthquake with respect to the distance to the trench for 2D model, 3D model with slip on the wider subduction segment, 3D model with slip on the narrower subduction segment (a) and the velocity 2 years after the earthquake over coseismic displacement with respect to the distance to the trench for 2D model, 3D model for the wider and narrower segments indicated in Fig. 15 (b).

As mentioned in Section 3, a zone of high viscosity is also imposed in a channel over the subduction interface below the seismic zone. The viscosity of this channel does not affect the results as long as it is sufficiently large. As we run this model for a long time, large deviatoric stresses progressively build up in the most viscous parts of the system, leading to long-term 'continuous' deformations. The

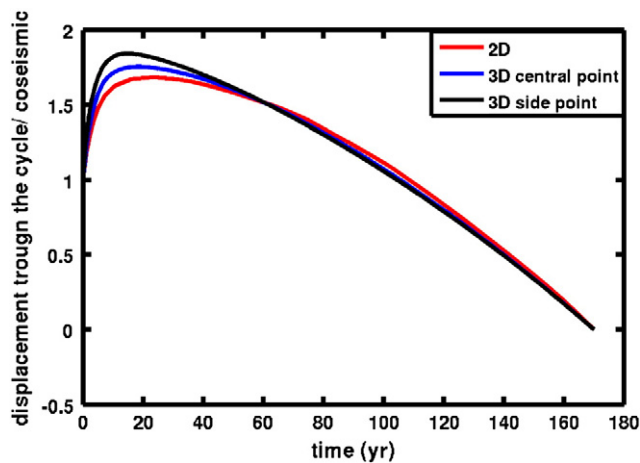


Fig. 17. Comparison of the horizontal displacement through the seismic cycle for 2D and 3D models at 700 km from the trench as functions of time during the seismic cycle. All 3 curves are normalised by the horizontal coseismic displacement.

system reaches a steady state. The continuous deformations induced by these large tectonic stresses plus the coseismic and postseismic deformations averaged over the seismic cycle induce no vertical motion and a continuous plate convergence. The case where steady state is not reached corresponds to cases with long-term 'tectonic' deformation in the system. Such long-term tectonic deformations are of course quite possible but will not be treated here. They are part of the general problem of forces and stresses in a subduction environment which is a rather controversial issue beyond the subject of the present paper. We are here interested in the cyclic part of the signal.

A mathematical equivalent of this "realistic model" is the rather classical "viscoelastic backslip" model (Fig. A1c) by Savage (1983). The principle of this model is simply to subtract from the 'realistic case' the motions uniform in time corresponding to the plate convergence: the velocities obtained in the 'realistic' case are considered as the superposition of continuous velocity plus a periodic motion (coseismic, postseismic and interseismic). In the backslip models, only the cyclic part is modelled. Of course, to achieve that, the continuous (in time) plate motion components must be subtracted from all the boundary conditions. So this model requires the imposed far field velocities to be equal to zero but a continuous aseismic slip must be applied along the subduction fault opposite to the imposed coseismic slip so that the long-term slip is zero.

The "realistic" and "viscoelastic backslip" models should be mathematically equivalent (as long as we use linear rheologies) because of the superposition principle. Indeed, we have checked numerically that the displacements during the earthquake cycle predicted by these 2 models are the same.

Taking into account the superposition principle, we propose a third technique – "superposition of N individual earthquakes" (Fig. A1d) which is more convenient for computations and at the same time gives the same result as the models discussed above.

The general idea is to impose only one earthquake, run the computation for a long time (i.e. observe the evolution of the system for the time $N \cdot T$, where T is a period of the cycle and N is the number of cycles) and then add the impact of the relaxation during each of N time series). The principle is illustrated by Fig. A2. The first step is to

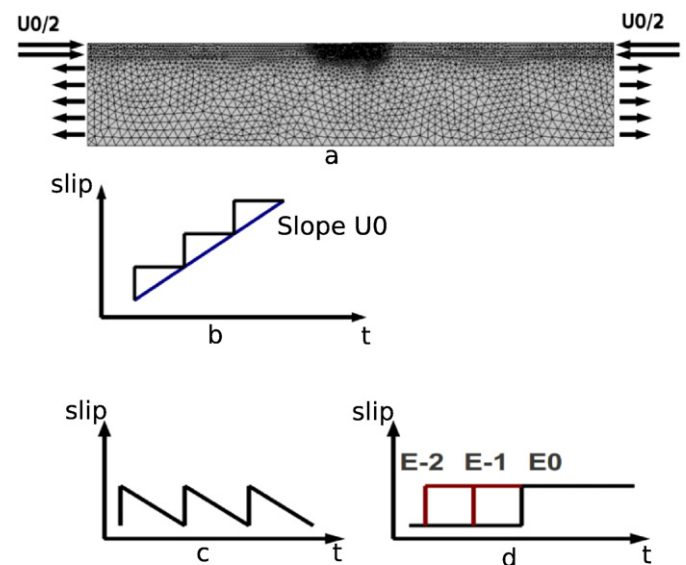


Fig. A1. (a) "Realistic" model – plate velocities imposed in the far-field and periodic earthquakes with the deformations predicted from elastic backslip model; (b) "Viscoelastic backslip" model – superposition of continuous velocity plus periodic motion; and (c) "Superposition of N individual earthquakes" model.

divide the displacement curve (blue), in N individual time intervals corresponding to the duration of a seismic cycle (Fig. A2a).

The second step (Fig. A2b) consists in adding together the curves corresponding to each segment (for example the green dot-dash curve Fig. A2b corresponds to the addition of the first and second segments of Fig. A2a, the blue dot-dash curve on Fig. A2b to the addition of the first, second and third segments and so on... until one gets the bottom black curve). By doing this, one adds the velocities due to past earthquakes which occurred at times t , $t+T$, $t+2T$...

The final step (Fig. A2c) is to take the linear trend which links the origin to the point at the end of the cycle and to subtract it from the black curve. The red curve is the answer to our problem: it shows the displacement during the seismic cycle with respect to the overriding plate.

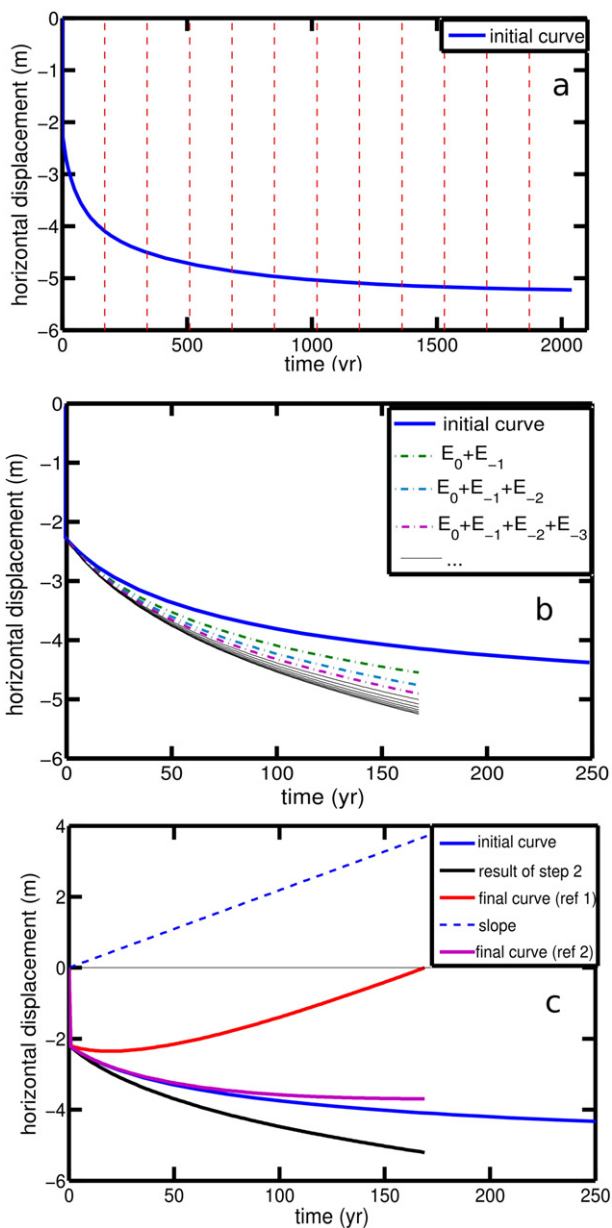


Fig. A2. Methodology of the “superposition model”: Step 1 (a) – to define individual intervals; Step 2 (b) – to add to the first interval the impacts of the other intervals; Step 3 (c) – to subtract the linear trend. Red curve is the horizontal displacement as function of time with respect to the overriding plate.

In the present paper, most computations have been done with this “superposition method”, and we checked against both other methods that it was indeed giving the same results. Because it is very simple, we believe that this “superposition method” will be very useful to compute interseismic velocities from past earthquake history in realistic 3D cases, where computation costs begin to be an issue.

Difference between post- and pre-seismic velocities

Note that it can be sometimes useful to compute the horizontal velocities after an earthquake, not in the referential of the overriding plate but in a referential moving at the local interseismic velocity (i.e. to use the measured difference between post- and interseismic velocities). Indeed, the GPS velocities are usually measured in the ITRF referential. In order to compare the results of our computation and the data, one needs to know the velocity of the overriding plate (in ITRF). But the notion of overriding plate velocity is sometimes fuzzy: we argue through this paper that in number of cases, overriding sub-plates or blocks proposed over the areas situated a few thousand kilometres away from highly coupled subduction zones have their measured GPS velocities highly polluted by the seismic cycle signal. So, often, one does not really know what is the ‘overriding plate velocity’. It can then be convenient to plot the difference of the velocities before and after the earthquake. Starting from the black curve on Fig. A2c, one just needs to subtract a linear trend (function *a.time*; dashed blue line on Fig. A2c) with a slope equal to the slope of the black curve at the end of the cycle and one gets the purple curve. It can be shown analytically and checked numerically that, at the beginning of the cycle, the blue initial signal linked to a single earthquake (represented on Fig. A2a, b and c) and the purple curve are superposed (the difference between the blue and purple curves is close to a quadratic function $c.time^2$ which brings back to zero the slope of the blue curve at the end of the cycle).

Appendix B. Short-term mantle rheologies

Since the proposed model features the asthenosphere with a viscoelastic rheology, it is important to choose the appropriate material behaviour. Maxwell viscoelastic model is often used for its simplicity. Its instantaneous response to a suddenly applied stress is purely elastic, while the following deformation is that of a Newtonian viscous fluid (constant strain rate if the deviatoric stress stays constant). It is characterised by two parameters: the elastic modulus μ_1 and the viscosity η_1 . But as shown by homogenization models (Ivins, 1996), a mixture of Maxwell materials is not a Maxwell material. The asthenosphere being not homogeneous, it has no reason to behave like a Maxwell material. Applying the self-consistent homogenization method to the case of the mantle, one finds that the mantle should rather be considered as a Burger body with a μ_2 equal to a few times (up to 10) μ_1 if one takes into account several scales of heterogeneities (pyroxene vs olivine, hotter and colder regions, more or less wet areas). In the present study, we use a Burger rheology (Fig. B1, right). The response of a Burger body to a sudden increase of stress is characterised by an instantaneous elastic reaction (μ_1), a long-term viscous flow (η_1) and fast transient creep (Kelvin–Voigt block with μ_2 which governs the total amplitude of the transient phase and η_2 the short-term viscosity). More elaborate shapes of the transient creep phase can be achieved by adding in series several Kelvin–Voigt elements (standard viscoelastic body). For simplicity,

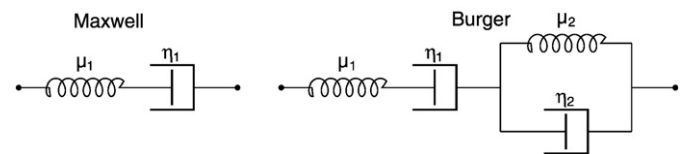


Fig. B1. Maxwell and Burger rheology models.

we will use here a basic Burger model, with only one Kelvin–Voigt element.

The parameters of the Burger model used here are based on our observations of post-seismic deformation in South-East Asia.

Acknowledgements

This work has been supported by the French ANR programs "Risques Naturels" and "Flash-Japan". The CINES centre has provided computer time in the phase of development of the 3D software. We thank P. Henry and an anonymous reviewer for their constructive suggestions which helped improving this paper.

References

- Ali, S.T., Freed, A.M., 2010. Contemporary deformation and stressing rates in southern Alaska. *Geophysical Journal International* 183, 557–571.
- Apel, E.V., Burgmann, R., Steblov, G., Vasilenko, N., King, R., Prytkov, A., 2006. Independent active microplate tectonics of northeast Asia from GPS velocities and block modeling. *Geophysical Research Letters* 33, L11303.
- Bock, Y., Prawirodirdjo, L., Genrich, J.F., Stevens, C.W., McCaffrey, R., Subarya, C., Puntodewo, S., Calais, E., 2003. Crustal motion in Indonesia from Global Positioning System measurements. *Journal of Geophysical Research* 108, B8.
- Bott, M.H.P., Dean, D.S., 1973. Stress diffusion from plate boundaries. *Nature* 243, 339–341.
- Chlieh, M., Avouac, J.P., Sieh, K., Natawidjaja, D.H., Galetzka, J., 2008. Heterogeneous coupling of the Sumatran megathrust constrained by geodetic and paleogeodetic measurements. *Journal of Geophysical Research* 113, B05305.
- Delescluse, M., Nicolas, C.R., Cattin, R., Fleitout, L., Trubienko, O., Vigny, C., 2012. April 2012 intraoceanic seismicity off Sumatra boosted by the Banda-Aceh megathrust. *Nature* 490, 240–244.
- Dragert, H., Hyndman, R.D., Rogers, G.C., Wang, K., 1994. Current deformation and the width of the seismogenic zone of the northern Cascadia subduction thrust. *Journal of Geophysical Research* 99, 653–668.
- Elsasser, W.M., 1969. Convection and stress propagation in the upper mantle. *Application of Modern Physics to the Earth and Planetary Interiors*, pp. 223–246.
- Fleitout, L., Garaud, J.D., Cailletaud, G., Vigny, C., Simons, W., Ambrosius, B., Trisirisatayawong, I., Satirapod, C., 2011. Modeling the post-seismic deformations of the Aceh, Nias and Benkulu earthquakes. *Geophysical Research Abstracts*, pp. EGU2011–EGU6503.
- Flück, P., Hyndman, R.D., Wang, K., 1997. Three-dimensional dislocation model for great earthquakes of the Cascadia subduction zone. *Journal of Geophysical Research* 103, 20,539–20,550.
- Freed, A.M., Bürgmann, R., Calais, E., Freymueller, J., Hreinsdóttir, S., 2006. Implications of deformation following the 2002 Denali, Alaska, earthquake for postseismic relaxation processes and lithospheric rheology. *Journal of Geophysical Research* 111, B01401.
- Heki, K., Miyazaki, S., Takahashi, H., Kasahara, M., Kimata, F., Miura, S., Vasilenko, N.F., Ivashchenko, A., An, K.D., 1999. The Amurian plate motion and current plate kinematics in eastern Asia. *Journal of Geophysical Research* 104, 29147–29155.
- Hetland, E.A., Hager, B.H., 2004. Relationship of geodetic velocities to velocities in the mantle. *Geophysical Research Letters* 31, L17604.
- Hu, Y., Wang, K., He, J., Klotz, J., Khazaradze, G., 2004. Three-dimensional viscoelastic finite element model for postseismic deformation of the great 1960 Chile earthquake. *Journal of Geophysical Research* 109, B12403.
- Ivins, E.R., 1996. Transient creep of a composite lower crust. 2. A polymineralic basis for rapidly evolving postseismic deformation modes. *Journal of Geophysical Research* 101, 28005–28028.
- Jin, S., Park, P.H., Zhu, W., 2007. Micro-plate tectonics and kinematics in northeast Asia inferred from a dense set of GPS observations. *Earth and Planetary Science Letters* 257, 486–496.
- Le Pichon, X., Mazzotti, S., Henry, P., Hashimoto, M., 1998. Transient and permanent deformation of central Japan estimated by GPS: 2. Strain partitioning and arc–arc collision. *Geophysical Journal International* 134, 501–514.
- Mazzotti, S., Pichon, X.L., Henry, P., Miyazaki, S.I., 2000. Full interseismic locking of the Nankai and Japan–west Kurile subduction zones: an analysis of uniform elastic strain accumulation in Japan constrained by permanent GPS. *Journal of Geophysical Research* 105, 13159–13177.
- Melosh, H.J., Fleitout, L., 1982. The earthquake cycle in subduction zones. *Geophysical Research Letters* 9 (1), 21–24.
- Melosh, H.J., Raefsky, A., 1981. A simple and efficient method for introducing faults into finite element computations. *Bulletin of the Seismological Society of America* 71, 1391–1400.
- Melosh, H., Raefsky, A., 1983. Anelastic response of the Earth to a dip slip earthquake. *Journal of Geophysical Research* 88, 515–526.
- Michel, G.W., Yu, Y.Q., Zhu, S.Y., Reigber, C., Becker, M., Reinhart, E., Simons, W., Ambrosius, B., Vigny, C., Chamot-Rooke, N., Pichon, X.L., Morgan, P., Mattheussen, S., 2001. Crustal motion and block behaviour in SE-Asia from GPS measurements. *Earth and Planetary Science Letters* 187, 239–244.
- Miura, S., Takahashi, N., Nakanishi, A., Tsuru, T., Kodaira, S., Kaneda, Y., 2005. Structural characteristics off Miyagi forearc region, the Japan trench seismogenic zone, deduced from a wide-angle reflection and refraction study. *Tectonophysics* 407, 165–188.
- Nostro, C., Piersanti, A., Antonioli, A., Spada, G., 1999. Spherical versus flat models of coseismic and postseismic deformations. *Journal of Geophysical Research* 104, 13,115–13,134.
- Okada, Y., 1985. Surface deformation due to shear and tensile faults in a half-space. *Bulletin of the Seismological Society of America* 75, 1135–1154.
- Panet, I., Mikhailov, V., Pollitz, F., Diament, M., Banerjee, P., Grijalva, K., 2000. Upper mantle rheology from GRACE and GPS post-seismic deformations after the 2004 Sumatra–Andaman earthquake. *Geochemistry, Geophysics, Geosystems* 11.
- Peacock, S.M., Hyndman, R.D., 1999. Hydrous minerals in the mantle wedge and the maximum depth of subduction thrust earthquakes. *Geophysical Research Letters* 26, 2517–2520.
- Piersanti, A., Spada, G., Sabadini, R., Bonafede, M., 1995. Global postseismic deformation. *Geophysical Journal International* 120, 544–566.
- Pollitz, F.F., 1997. Gravitational viscoelastic postseismic relaxation on a layered spherical Earth. *Journal of Geophysical Research* 102, 17,921–17,941.
- Pollitz, F., Bürgmann, R., Romanowicz, B., 1998. Viscosity of oceanic asthenosphere inferred from remote triggering of earthquakes. *Science* 280, 1245.
- Pollitz, F., Roland, B., Paramesh, B., 2006. Post-seismic relaxation following the great 2004 Sumatra–Andaman earthquake on a compressible self-gravitating Earth. *Geophysical Journal International* 167, 397–420.
- Pollitz, F., Banerjee, P., Grijalva, K., Nagardjan, B., Bürgmann, R., 2008. Effect of 3-D viscoelastic structure on post-seismic relaxation from the 2004 M=9.2 Sumatra earthquake. *Geophysical Journal International* 173, 189–204.
- Satirapod, C., Trisirisatayawong, I., Fleitout, L., Garaud, J., Simons, W., 2012. Vertical motions in Thailand after the 2004 Sumatra–Andaman Earthquake from GPS observations and its geophysical modelling. *Advances in Space Research* <http://dx.doi.org/10.1016/j.asr.2012.04.030>.
- Savage, J.C., 1983. A dislocation model of strain accumulation and release at a subduction zone. *Journal of Geophysical Research* 88, 4984–4996.
- Savage, J.C., Prescott, W.H., 1978. Asthenosphere readjustment and the earthquake cycle. *Journal of Geophysical Research* 83, 3369–3376.
- Savage, J.C., Svarc, J.L., Prescott, W.H., Murray, M.H., 2000. Deformation across the forearc of the Cascadia subduction zone at Cape Blanco, Oregon. *Journal of Geophysical Research* 105, 3095–3102.
- Shestakov, N.V., Gerasimenko, M.D., Takahashi, H., Kasahara, M., Bormotov, V.A., Bykov, V.G., Kolomiets, A.G., Gerasimov, G.N., Vasilenko, N.F., Prytkov, A.S., Timofeev, V.Y., Ardyukov, D.G., Kato, T., 2010. Present tectonics of the southeast of Russia as seen from GPS observations. *Geophysical Journal International* 184, 529–540.
- Simoes, M., Avouac, J.P., Cattin, R., Henry, P., 2004. The Sumatra subduction zone: a case for a locked fault zone extending into the mantle. *Journal of Geophysical Research* 109, B10402.
- Simons, W.J.F., Socquet, A., Vigny, C., Ambrosius, B.A.C., Haji Abu, S., Promthong, C., Subarya, C., Sarsito, D.A., Matheussen, S., Morgan, P., Spakman, W., 2007. A decade of GPS in Southeast Asia: resolving Sundaland motion and boundaries. *Journal of Geophysical Research* 112, B06420.
- Tanaka, A., Yamano, M., Yano, Y., Sasada, M., 2004. Geothermal gradient and heat flow data in and around Japan (i): appraisal of heat flow from geothermal gradient data. *Earth, Planets and Space* 56, 1191–1194.
- Thatcher, W., Rundle, J.B., 1979. A model for the earthquake cycle in underthrust zones. *Journal of Geophysical Research* 84, 5540–5556.
- Thatcher, W., Rundle, J.B., 1984. A viscoelastic coupling model for the cyclic deformation due to periodically repeated earthquakes at subduction zones. *Journal of Geophysical Research* 89, 7631–7640.
- Uchida, N., Kirby, S.H., Okada, T., Hino, R., Hasegawa, A., 2010. Supraslab earthquake clusters above the subduction plate boundary offshore Sanriku, northeastern Japan: seismogenesis in a graveyard of detached seamounts? *Journal of Geophysical Research* 115, B09308.
- Vigny, C., Simons, W.J.F., Abu, S., Bamphenyu, R., Satirapod, C., Choosakul, N., Subarya, C., Socquet, A., Omar, K., Abidin, H.Z., Ambrosius, B.A.C., 2005. Insight into the 2004 Sumatra–Andaman earthquake from GPS measurements in southeast Asia. *Nature* 436, 201–206.
- Wang, K., He, J., Dragert, H., James, T.S., 2001. Three-dimensional viscoelastic interseismic deformation model for the Cascadia subduction zone. *Earth Planets Space* 53, 295–306.
- Wang, K., Hu, Y., He, J., 2012. Deformation cycles of subduction earthquakes in a viscoelastic earth. *Nature* 484, 327–332.
- Yamamoto, Y., Hino, R., Nishino, M., Yamada, T., Kanazawa, T., Hashimoto, T., Aoki, G., 2006. Three-dimensional seismic velocity structure around the focal area of the 1978 Miyagi–Oki earthquake. *Geophysical Research Letters* 33, L10308.
- Zienkiewicz, O.C., Taylor, R.L., 2000. *The finite element method*, 5th ed. Solid Mechanics, vol. 2. Butterworth-Heinemann.
- Z-set, 2011. Z-set/Zébulon: Material and structure analysis suite. <http://www.zset-software.com/>.